Soft Matter

REVIEW

View Article Online
View Journal | View Issue

Cite this: *Soft Matter*, 2022, **18**, 4823

From vesicles toward protocells and minimal cells

Masayuki Imai, *[a] Yuka Sakuma, [a] Minoru Kurisu [a] and Peter Walde [b]

In contrast to ordinary condensed matter systems, ''living systems'' are unique. They are based on molecular compartments that reproduce themselves through (i) an uptake of ingredients and energy from the environment, and (ii) spatially and timely coordinated internal chemical transformations. These occur on the basis of instructions encoded in information molecules (DNAs). Life originated on Earth about 4 billion years ago as self-organised systems of inorganic compounds and organic molecules including macromolecules (*e.g.* nucleic acids and proteins) and low molar mass amphiphiles (lipids). Before the first living systems emerged from non-living forms of matter, functional molecules and dynamic molecular assemblies must have been formed as prebiotic soft matter systems. These hypothetical cell-like compartment systems often are called ''protocells''. Other systems that are considered as bridging units between non-living and living systems are called ''minimal cells''. They are synthetic, autonomous and sustainable reproducing compartment systems, but their constituents are not limited to prebiotic substances. In this review, we focus on both membrane-bounded (vesicular) protocells and minimal cells, and provide a membrane physics background which helps to understand how morphological transformations of vesicle systems might have happened and how vesicle reproduction might be coupled with metabolic reactions and information molecules. This research, which bridges matter and life, is a great challenge in which soft matter physics, systems chemistry, and synthetic biology must take joined efforts to better understand how the transformation of protocells into living systems might have occurred at the origin of life.

Received 30th November 2021,
Accepted 2nd June 2022

DOI: 10.1039/d1sm01695d

rsc.li/soft-matter-journal

1. Introduction

1.1. Living systems

Although it is difficult to formulate a generally accepted definition of ''life'', all living entities exist on the basis of

[a] *Department of Physics, Graduate School of Science, Tohoku University, 6-3 Aoba, Aramaki, Aoba, Sendai 980-8578, Japan. E-mail: imai@bio.phys.tohoku.ac.jp*
[b] *Department of Materials, ETH Zürich, Vladimir-Prelog-Weg 5, CH-8093 Zürich, Switzerland*

Masayuki Imai

Masayuki Imai is a Prof. of Physics at Tohoku University, Japan. After his doctoral thesis in the group of Prof. Keisuke Kaji at Kyoto University, he joined the neutron scattering group at the University of Tokyo, where he worked on the application of small angle neutron scattering for soft matter research. After leading the experimental soft matter physics group at Ochanomizu University, he was appointed professor at Tohoku University in 2012. His main research interests are in soft matter physics approaches to living systems, minimal cells, protocells and the morphogenesis in multicellular systems.

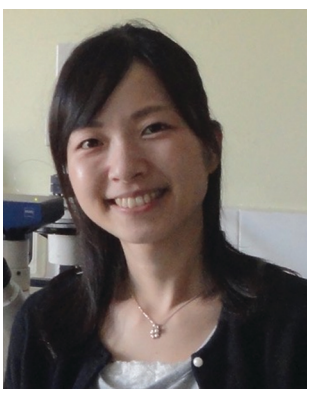

Yuka Sakuma

Yuka Sakuma is a lecturer at Tohoku University in Japan. She received her doctorate degree of Science in 2010 from Ochanomizu University, Japan under supervision of Prof. Masayuki Imai. Her main research is reproducing cellular functions with simple lipid vesicles and understanding how life controls their functions from soft matter physics point of view. Recently she has focused on the difference in membrane fluidity between artificial cells and living cells using her original viscosity measurement technique.

fundamentally identical principles. While living systems can be of an apparently extraordinary diversity, all forms of life are (i) based on cells as fundamental units of life, and (ii) generate copies of themselves by taking chemical substances and energy from their surroundings for their reproduction.[1] Cell reproduction is based on instructions encoded in information molecules (DNAs) that are localized within the cells; cells are highly sophisticated membrane-bound compartment systems that consist of a very complex network of spatially and timely controlled chemical transformations (metabolism), even in the case of a seemingly simple bacterium. In addition to a large number of different low molar mass organic and inorganic compounds, all biological cells contain structurally complex macromolecules with specific functions, such as nucleic acids and proteins (enzymes), and a complex mixture of self-assembled amphiphilic molecules that are, for example, part of the plasma membrane that exists in all cells and separates the cell interior from other living cells or from a non-living environment. One of the great challenges of cell biology,[1] systems chemistry,[2–4] soft matter physics,[5–7] and origin-of-life[8,9] research is to elucidate the likely pathway(s) that led from non-living forms of matter to an autonomous and sustainable reproducing compartment system that might have been formed as precursor system, which then transformed into the first living cells. The hypothetical precursor systems which are thought to have formed in prebiotic times before the first cells emerged are often called "protocells".[10–15] Such hypothetical protocells consisted of molecules present in prebiotic times. Another approach towards understanding the emergence of the first cells is to consider – and try to build – "minimal cells". They resemble biological cells in their minimal form, *i.e.*, they are assembled membrane-bounded compartment systems that show autonomous and sustainable reproduction of the entire systems, but their constituents are not limited to prebiotic substances. Both protocells and minimal cells must contain the essence of living systems (at least partly), as schematically represented in Fig. 1. This review aims to shed light on the road from vesicle to protocells and minimal cells from a soft matter physics point of view.

The key question many scientists and philosophers have asked for decades is how to "extract" the essence of a living system. Gánti proposed the "chemoton" (Fig. 1a), a model of a living biological cell, by considering three autocatalytic cycles: a metabolic cycle, a genetic cycle and a membrane cycle.[16–19] Here, ingredients (X) taken in from the environment are converted into membrane precursor molecules (T'') through intermediates (A_i) in the metabolic cycle, and waste molecules (Y) are excreted. In the genetic cycle, the genetic polymer (pV_n) is template-replicated, and a membrane precursor molecule (R) is simultaneously synthesised from a product (V') of the metabolic cycle. In the membrane cycle, the membrane molecule T is synthesised from T'' and R, which is then supplied to the membrane to realize the proliferation of the system. On the other hand, from a contemporary living cell point of view, ~250 essential genes have been identified in one of the simplest known bacterium, *Streptococcus sanguinis*; an essential gene is defined as one whose loss is lethal.[20,21] The identified essential genes are associated with only three basic categories of biological functions ("domains") (Fig. 1b): (1) the "energy production domain", which is involved in the synthesis of "energy currency molecules" from glucose taken in from the environment (grey); (2) the "processing of genetic information domain", which is in charge of replicating DNA (*i.e.*, the macromolecular information molecule), and of synthesising proteins *via* RNA (green); and (3) the "maintenance of the cell membrane domain", in which proteins catalyse the synthesis of membrane molecules from by-products of the energy production domain using energy currency molecules (blue). The final products, membrane molecules, are incorporated into the cell membrane, which results in membrane growth and cell division, *i.e.*, cell proliferation. This conceptual overview of the

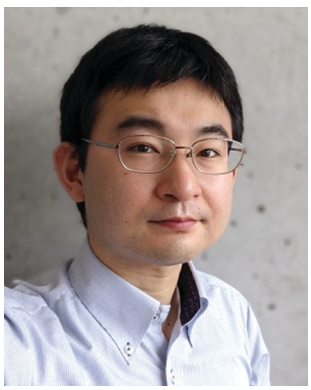

Minoru Kurisu

Minoru Kurisu studied Physics at Tohoku University, Japan. For his doctorate study, he joined the group of Prof. Masayuki Imai at Tohoku University. He worked on the experimental construction and physical analysis of a synthetic minimal cell system where vesicle growth and division is coupled with a membrane surface-confined polymerisation reaction. During his doctorate study, he visited the group of Prof. Peter Walde at ETH Zürich to study chemical techniques on polymerisation reactions and enzymes. He received his doctorate degree in Physics in 2022 from Tohoku University. He is currently a Research Associate in the group of Prof. Masayuki Imai.

Peter Walde

Peter Walde studied chemistry at the ETH Zurich, Switzerland. He completed his doctoral thesis at ETH Zurich in 1983 (under the supervision of Prof. Pier Luigi Luisi). After postdoctoral stays in New Zealand at the University of Auckland (Prof. Charmian O'Connor) and in Japan at the University of Nagasaki (Prof. Junzo Sunamoto), he returned to ETH Zurich in 1986, where he remained until his official retirement at the end of 2021. His research interests in the Department of Materials at ETH included various fundamental and applied aspects of vesicles as well as the preparation and application of polymer-enzyme conjugates.

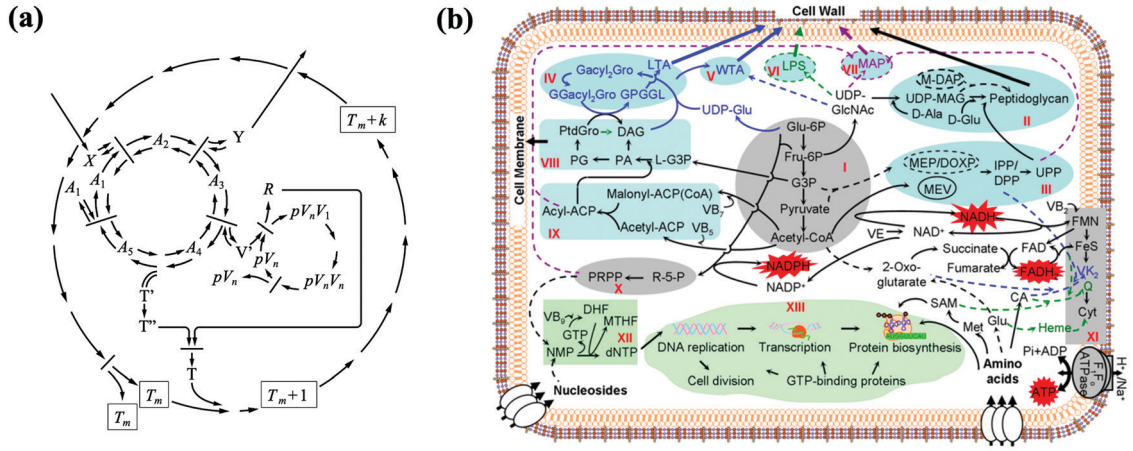

Fig. 1 (a) Gánti's chemoton model of a living system. Three self-producing subsystems are coupled stoichiometrically: Metabolic cycle $A \rightarrow 2A$, Genetic cycle $pV_n \rightarrow 2pV_n$ and Membrane cycle $T_m \rightarrow 2T_m$. This coupling results in compartment (cell) proliferation, see text for details. (Reprinted with permission from T. Gánti, *J. Theor. Biol.*, 1997, **187**, 583–593. Copyright 1997 Academic Press Limited. The characters were enlarged to make them more readable.) (b) Deduced essential pathways based on an analysis of the essential genes of the bacterium *S. sanguinis*. The three functions associated with essential pathways are indicated by different colors: blue, maintenance of the cell membrane; gray, energy production; green, processing of genetic information. (Reprinted with permission from P. Xu *et al.*, *Sci. Rep.*, 2011, **1**, 125, Copyright 2011 Springer Nature.)

functioning of a unicellular organism, a bacterium, supports the chemoton model. It is worth noting that in the "processing of genetic information domain", the transfer of sequence information from nucleic acids to proteins is possible, but sequence transfer from proteins to nucleic acid sequences is impossible (known as the central dogma of molecular biology).[1,22] Therefore, DNA sequences coding for proteins that participate in the synthesis of the most adaptive membrane molecules against the environment will survive as a result of competitive advantage (Darwin's theory of biological evolution by natural selection). In this context, the seminal paper by Szostak, Bartel, and Luisi is worth mentioning: the authors argued that the realization of the coupling between a vesicle-entrapped RNA replicase (a ribozyme) and vesicle compartment reproduction would mean a first step towards the synthesis of a living system, *i.e.*, synthesising life.[23] Stimulated by this paper, various approaches have been undertaken with the aim of making progress in understanding the origin of life on the basis of a coupling of RNA chemistry and compartmentalization; several books and review articles have been published on this fascinating topic.[24–49] However, despite various theories and experimental demonstrations of potentially prebiotic syntheses of organic molecules that are essential building blocks of nucleic acids and proteins, one has to be modest in terms of the progress that has been made towards understanding the emergence of the first cells from the non-living at the origin of life. It is a great challenge to develop information molecule-containing chemical non-equilibrium compartment systems that are not only able to grow and divide but also have the capability to mutate and to grow and divide in a mutated state so that one would call them "living". So far, this has not been achieved (yet).

1.2. Approaches to living systems

According to the general features of the membrane-bound life model systems mentioned above, a key toward a better understanding of the transformation of molecules and molecular assemblies into living systems involves scenarios about (i) the type and/or origin of information molecules, (ii) the establishment of a metabolic network to synthesise membrane molecules based on the instructions by the information molecules, and (iii) the growth and division of membranous compartments by using the synthesised membrane molecules. It is unclear whether these three processes were already linked at the stage of the origin of life, they appear essential for achieving a stable living system.

In many previous origin-of-life research works, the main focus was on the origin of information molecules, known as the RNA world scenario.[50–53] Various reaction schemes have been proposed for the prebiotic synthesis of nucleobases, nucleotides, and RNA, as the first genetic information molecule, from ingredients that existed in the Hadean eon.[39,54–59] Here it should be noted that in order to synthesise such information-carrying macromolecules in the hydrosphere of the primitive Earth, a very dilute solution of prebiotic precursor molecules (monomers) must have been concentrated to react (the "concentration problem").[60,61] Mineral surfaces,[62] hot springs[63] and hydrothermal vents[64] of the primitive Earth are candidates for the required intermolecular condensation reactions to take place efficiently. In particular, it has been shown that the polymerization of oligonucleotides can proceed due to a coupling of thermal convection and thermophoresis in the vicinity of hydrothermal vents.[61,65,66] A more complex condensation coupled with phase separation of polyions is the coacervate model, which will be described below.

Functional RNA requires a high degree of oligo- or polymerization to encode sufficient information for maintaining a living system. At the same time, a long RNA sequence requires sophisticated reaction mixtures that prevent replication errors (the "error catastrophe").[67] Eigen proposed a hypercycle which is a closed reaction network consisting of self-replicating entities

connected by a catalytic loop. The hypercycle removes erroneous products using a catalytic cascade network and shows a hyperbolic growth rate,[68,69] which might solve the error catastrophe problem. Recently, Toyabe *et al.* proposed a templated ligation model, which leads to a cascade of enhanced template binding and fast ligation reactions (nonlinear growth).[70] Exponential growth leads to a selection of the globally "fittest" species, *i.e.*, to Darwinian evolution, whereas nonlinear growth results in a "once-for-ever" selection. So far, the evolution of RNA has been examined based on the fitness landscape concept[71,72] theoretically[73,74] and experimentally.[75,76] A big challenge is to link the chemical requirements for RNA synthesis with the physical requirements for acting as information molecules.[58,59]

A simple scenario for coupling membrane growth with potentially prebiotic molecules is as follows. It is assumed that primitive membrane molecules (*e.g.* fatty acids),[45,77–81] amino acids, peptides[82–85] and RNA were present on the early Earth due to chemical synthesis (for example, in high-temperature geochemical niches), or some of these molecules were delivered to the Earth *via* carbonaceous meteorites.[11] It is further assumed that such primitive molecules coexisted in the "primordial soup".[86] Mixtures of polyanions and polycations in the primordial soup may have undergone phase separation (formation of dynamic coacervate droplets in a dilute aqueous medium) due to a balance between electrostatic and/or hydrophobic interactions and configurational entropy.[5,87] If really formed, such coacervate droplets (usually micrometre-sized) did not have a membrane but were membrane-less compartments. Depending on the type of coacervate, *i.e.*, the molecular composition, it was shown in laboratory experiments that coacervates can concentrate prebiotically relevant molecules, such as amino acids, peptides, lipids, nucleotides, and RNA, which encourage RNA polymerization and ribozyme catalytic activity,[88,89] thereby promoting metabolic reactions.[90,91] In addition, fatty acids encapsulated in coacervates show a transition from membrane-free compartmentalisation to membrane-bound compartmentalisation.[92–94] Interestingly, coacervate droplets show growth, fusion, and division under assumed primordial conditions, *i.e.*, reproduction of membrane-free coacervates as protocell models.[95] Membrane-bound protocells might be generated from these and/or other relevant processes.

Compartmentalisation is a key feature of all forms of life today, with membrane-bound cells being the fundamental units of any living system (Fig. 1). In this review, we consider a scenario in which functionalized vesicles preceded the first living cells. In other scenarios, micelles[96,97] or coacervates[47,98–100] are considered as pre-cellular compartment systems. It may well be that in prebiotic times all three types of molecular assembly systems once played important roles. The focus in this review is on vesicles only.

Membrane-forming molecules are thought to have self-assembled to form aggregates,[101,102] including vesicles, and to have played a central role in prebiological compartment reproduction. It is assumed that protocellular vesicles underwent growth and division processes (Fig. 2a) by incorporating membrane molecules with the aid of amino acids and peptides present in the primordial soup.[11,31,103–105] If RNA molecules played an important role in this scenario, it is currently difficult to understand how a metabolic reaction system in which RNA molecules and catalytically active proteins were linked to promote the synthesis of membrane molecules. What could have happened is that RNA molecules developed into ribozymes that functioned as catalysts,[106] to promote ribozyme-catalysed RNA polymerisation[107] and ribozyme self-replication.[108] However, for catalysing sophisticated reaction pathways that lead to the synthesis of membrane molecules, peptides and proteins (built from a set of 20 chemically different amino acids) appear to be more suitable than RNA molecules, which consist of at most only four chemically different bases. Nevertheless, following the "RNA world scenario", ribozymes that catalyse tRNA aminoacylation[109] and peptide synthesis,[110] which link RNA and proteins, must have emerged at some stage. Such RNA-mediated protein synthesis system eventually might have generated a metabolic network, as sketched in the chemoton model (Fig. 1a), whereby some of the proteins acted as catalysts to synthesise membrane molecules.[97,111–113] However, to form a metabolic reaction network as shown in Fig. 1b, the reaction products must have mutually catalytic relationships (the requirement for "autocatalytic sets"), and the reaction paths must have been connected to form a closed reaction network ("percolation transition").[114,115] Of particular interest for metabolic evolution are so-called "reflexively autocatalytic food-generated networks (RAFs)" in which each reaction is catalysed by a molecule from within the network, and all molecules can be produced from a set of food molecules by the network itself.[116,117]

In a contemporary cell, the membrane molecules synthesised in the metabolic network are incorporated into the cell membrane as shown in Fig. 1b, and in the case of dividing cells, the cell membrane grows and divides to produce an offspring. This offspring completes the cell cycle by recovering the original area and volume of the parent cell. Since cell membranes consisting of amphiphilic molecules provide a heterogeneous chemical reaction field[118,119] and govern cell proliferation by morphological transitions, the likely importance of membranes in the origin of life was discussed and investigated extensively in the past.[11,13,31,32,37,41,46,120] In one scenario, for example, it is assumed that in the primordial soup numerous types of amphiphilic molecules coexisted and formed molecular assemblies having various compositions. Some of these assemblies may have incorporated amphiphilic molecules from the external solution through specific interactions, resulting in growth and division of the assemblies. After many growth and division cycles, the assembly with the composition that gave the fastest division rate survived, resembling a pre-Darwinian evolution by transferring assembly composition information.[120–122]

Although typical previous studies on protocells considered the reproduction of fatty acid-based vesicles through vesicle membrane growth and division, it is also possible to attain vesicle reproduction by vesicle-oil droplet transformations.[123] Fatty acid vesicles transform into oil droplets either by decreasing the pH or by increasing the temperature (with concomitant release of the vesicle content). This process is reversible so that fatty acid vesicles can form again upon pH increase or temperature decrease to the

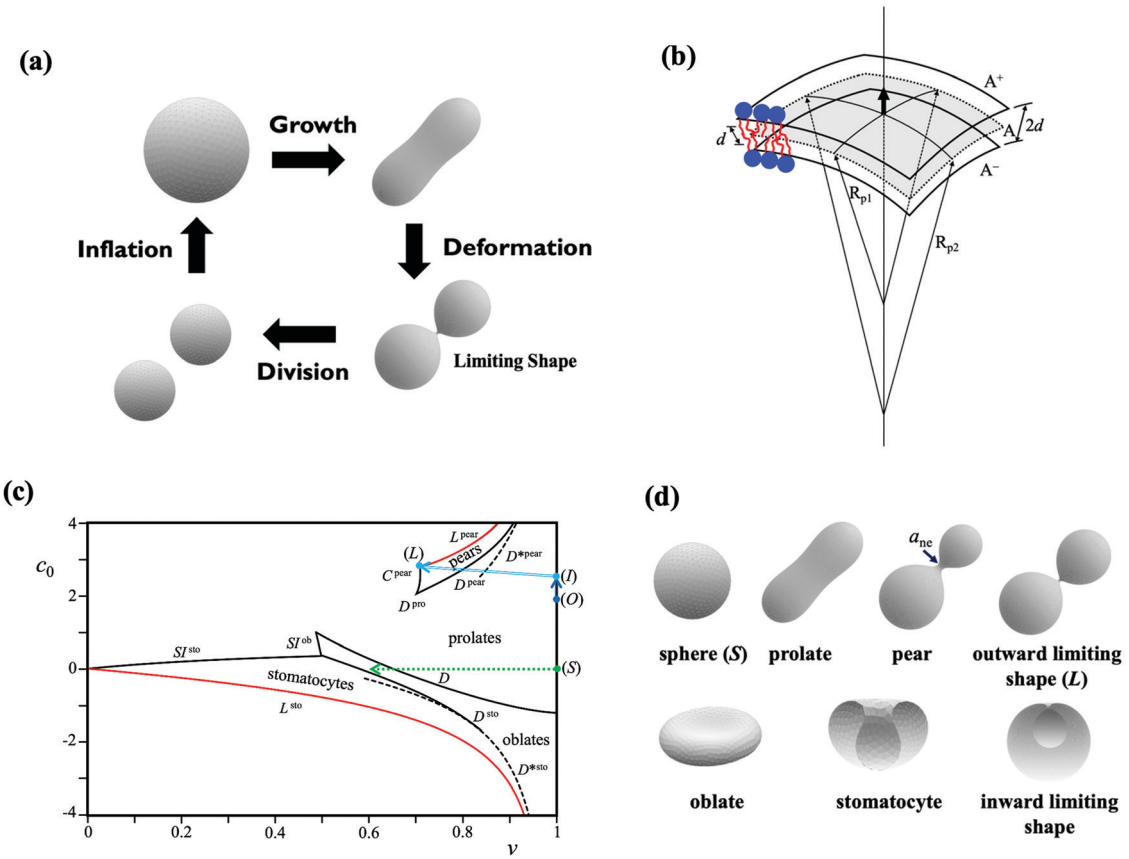

Fig. 2 (a) Illustration of a vesicle reproduction cycle consisting of four steps: membrane growth and shape change, vesicle deformation to a limiting shape, vesicle division, and inflation of the divided vesicles to the size of the initial vesicle. Here, basic components that constitute the vesicle reproduction process are presented as plausible reproduction model, which may deviate from the real cell proliferation cycle. (b) Geometry of a curved bilayer. The surface area A is the area at the bilayer midplane. The principal curvatures, $C_1 = 1/R_{p1}$ and $C_2 = 1/R_{p2}$, are the maximum and minimum values of curvatures, which are defined at the bilayer midplane. The thick arrow indicates the normal vector. A^+ and A^- are the neutral surfaces of the outer and inner leaflets, respectively. The distance between the neutral surfaces of the two leaflets is denoted by d. (c) Phase diagram based on the spontaneous-curvature model. This phase diagram shows the shape of lowest bending energy for a given reduced spontaneous curvature c_0 and reduced volume v. The regions where the prolates, pears, oblates, and stomatocytes have lowest energy are separated by transitions. The line L^{pear} denotes where budding occurs (outward limiting shape) and the line L^{sto} corresponds to the inclusion of a spherical cavity (inward limiting shape). The line C^{pear} denotes a continuous transition. All other transitions, D^{pear}, D^{pro}, D, and D^{sto}, are discontinuous. The dashed lines D^{*pear} and D^{*sto} denote approximations to the discontinuous transition. Beyond the lines SI^{ob} and SI^{sto}, there are states where different parts of the vesicle membrane come into contact. The green dotted arrow indicates the deformation pathway for a spherical vesicle with $c_0 = 0$ (S), which does not lead to vesicle reproduction. The light blue arrow indicates a deformation pathway of a spherical vesicle ($v = 1$) having $c_0 = 2.6$, which deforms from (I) to a symmetric limiting shape (L) ($v = 0.71$) by increasing the vesicle surface area at constant volume. After division, the offspring spherical vesicle has $c_0 = 2$ and $v = 1$ (O), which swells to (I) by the inflation process (dark blue arrow). This (I) → (L) → (O) → (I) cycle is a vesicle reproduction cycle. (Reprinted with permission from U. Seifert *et al.*, *Phys. Rev. A*, 1991, **44**, 1182–1202. Copyright 1991 The American Physical Society, Two limiting shape lines are highlighted with red colour; the green dotted arrow and the blue arrows were added to show the deformation pathway discussed in the text). (d) Typical shapes based on the spontaneous-curvature model; sphere, prolate, pear with a lipidic neck connecting two spheres (a_{ne}: neck radius), outward limiting shape, oblate, stomatocyte, and inward limiting shape.

conditions under which stable vesicles form. After such vesicle reassembly process, the aqueous content of the vesicles will be different from that before the vesicle-droplet transformation.[123] This reversible vesicle-oil droplet transition with reshuffling the content is a way of transporting solutes between the interior of the vesicles and the external medium and *vice versa*. This purely physical process is unique for simple amphiphiles (like fatty acids) and certainly worth considering when further developing fatty acid-based vesicles as protocell model systems.

Artificial vesicles (prepared from biological or synthetic amphiphiles) are a well-defined model system for studying basic properties of cell membranes. Especially, the physico-chemical properties that determine vesicle shape are now well understood from theoretical,[124–131] and experimental[132–136] points of view. This is largely due to efforts in the field of biomembrane physics (a branch of soft condensed matter physics).[137] Applying this knowledge for understanding the growth and division of artificial vesicles will help to understand the physical requirements that must have been fulfilled in prebiotic times if vesicles existed as protocellular compartment systems and if these vesicles developed into self-reproducing compartments.

In the following, we will summarize concepts and results of theoretical, experimental, and simulation studies focusing on the reproduction of vesicles as models of protocells and for the preparation of "minimal cells". Concerning protocells, the experimental examples given are by no means examples involving potentially prebiotic molecules only. More important is to summarise what has been archived so far and how experimental results are linked to theoretical considerations. First, we will explain the membrane elasticity theory for vesicle reproduction and then discuss the simplest form of a vesicle reproduction cycle consisting of (i) vesicle membrane growth, (ii) vesicle deformation to a limiting shape (two spherical vesicles connected by a very narrow membrane neck), (iii) vesicle division, and (iv) vesicle inflation that is required at different stages of the entire cycle (Fig. 2a). Finally, we will discuss the interplay among information molecules, metabolism, and reproduction of vesicles to construct experimental vesicular protocell models or even "minimal cells".

2. Reproduction of vesicles

2.1. Growth and division of prokaryotic cells

The realisation of vesicle reproduction coupled with a metabolic reaction network is an important milestone on the pathway from molecular assemblies to living systems. Unfortunately, how such a vesicle reproduction system arose in a prebiotic environment is still a mystery. One possible approach to achieve vesicle reproduction in laboratory experiments is to mimic growth and division in prokaryotic cells, *i.e.*, bacteria.[1] Here, we overview the mechanisms of growth and division of prokaryotic cells. As shown in Fig. 1b, the synthesis of membrane molecules is carried out by starting from glycero-3-phosphate (G3P) and pyruvate, which are by-products of glycolysis. Pyruvate is converted into long-chain fatty acids (acyl-CoAs) *via* acetyl-CoA. The membrane enzyme glycerol-3-phosphate acyltransferase (GPAT) catalyses the synthesis of lysophosphatidic acids (LPAs) by a specific reaction between acyl-CoA and G3P. A second long-chain fatty acid (acyl-CoA) is then regioselectively bonded to LPA, resulting in the formation of phosphatidic acid (PA), which has two hydrophobic acyl chains. Enzymes catalyse the modification of the hydrophilic head group of PA to obtain various types of 1,2-diacyl glycerophospholipids such as phosphatidylethanolamines (PEs), phosphatidylcholines (PCs), and phosphatidylserines (PSs). The initial steps of phospholipid synthesis are carried out in the cytoplasm,[138] up to the synthesis of fatty acids, which are then transported to the cell membrane, where conversion into phospholipids takes place, causing the growth of the cell membrane.

In the division process of bacteria, first the circular DNA is replicated and separated into two regions within the cell, and then a protein called FtsZ appears at the division site to form a ring-shaped assembly, the Z-ring. The contraction of this Z-ring causes the bacterial cell to divide.[139,140] Concerning the growth and division of protocells and very early cells (early "primitive forms of life"), however, such a protein-based division system appears unlikely since it involves complex macromolecules that most probably did not exist in prebiotic time. Therefore, it is likely that simpler division mechanisms were in operation in compartment systems that preceded the first cells (protocells), or they were even operating in very early forms of life. The division mode of bacteria called "L-form" that is not mediated by FtsZ[141,142] may give some hint about the division mechanism of very early cells and of vesicular protocells.[143] The proliferation of "L-form" cells does not require a complex protein regulation but simply utilises the physico-chemical properties of the cell membrane.

2.2. Membrane elasticity model of vesicle reproduction

The vesicle reproduction cycle consists of four stages; vesicle membrane growth, vesicle deformation to a limiting shape, vesicle division, and inflation (*i.e.*, filling the vesicles with aqueous solution to attain the size of the original vesicle), see Fig. 2a. Please note that the reproduction cycle shown in Fig. 2a does not necessarily represent the real cell proliferation cycle.

In this section, we explain the "membrane elasticity model" governing vesicle deformation and division. A simple model for describing vesicle deformation is the spontaneous curvature model derived by Helfrich,[124,144] in which the shape of a vesicle is determined by the minimization of the total elastic energy under the constraints on vesicle surface area A and vesicle volume V

$$F_{\mathrm{SC}} = \frac{\kappa}{2}\oint \mathrm{d}A(C_1 + C_2 - C_0)^2 + \kappa_{\mathrm{G}}\oint \mathrm{d}A C_1 C_2, \qquad (1)$$

where C_i (i = 1, 2) is the principal curvature of the membrane (the principal radii of curvature, $R_{p1} = 1/C_1$ and $R_{p2} = 1/C_2$, are the extremal values of radius of curvature, whereby for a bilayer membrane, the principal curvatures and surface area are defined at the bilayer midplane, see Fig. 2b), κ and κ_{G} are the bending rigidity and the Gaussian bending rigidity, respectively. C_0 is the spontaneous curvature originating from either a different chemical environment on both sides of the membrane, or a different chemical composition of the two monolayers, *i.e.*, asymmetry in the bilayer. The first term expresses the bending energy caused by vesicle deformation, and the second term expresses the Gaussian bending energy that depends only on the topology and does not depend on the shape of the vesicle. Due to the Gauss–Bonnet theorem[145] the second term is expressed by $\kappa_{\mathrm{G}}\oint \mathrm{d}A C_1 C_2 = 4\pi\kappa_{\mathrm{G}}(1-g)$, where g is the genus given by the number of handles (holes) of the vesicle surface (a spherical vesicle has genus 0, and a torus vesicle has genus 1). Without topology transition, such as vesicle division, the second term is constant. Thus, this term can be neglected for the vesicle deformation to the limiting shape, but it plays an important role in vesicle division. The vesicle deformation process can be described by two geometric parameters, (i) the reduced volume given by $v = V \Big/ \left[\left(\frac{4\pi}{3}\right)R_0^3\right]$, where $R_0 = \left(\frac{A}{4\pi}\right)^{1/2}$ is the radius of a sphere with the same surface area A as the deformed vesicle, and (ii) the reduced spontaneous curvature $c_0 = C_0 R_0$. The reduced volume is a measure of the volume/area ratio.

The phase diagram of the "spontaneous curvature model" using v and c_0 is shown in Fig. 2c[125] and typical shapes observed in the phase diagram are shown in Fig. 2d. In this phase diagram, the (outward) limiting shape vesicle is located on the line L^{pear}, where the vesicle membrane must have a specific reduced spontaneous curvature. At the left end of the line L^{pear}, the vesicle has a symmetric limiting shape, and as it moves to the right on the line L^{pear}, the limiting shape becomes asymmetric.

An area difference elasticity (ADE) model has been proposed based on the bilayer property of a unilamellar vesicle membrane. In unilamellar vesicles, the vesicle membrane (bilayer) is composed of an inner monolayer leaflet and an outer monolayer leaflet. This membrane can be characterised by an intrinsic parameter, the "preferred area difference", expressed by $\Delta A_0 = (N^+ - N^-)a_0$, where N^+ and N^- are the numbers of membrane molecules in the outer and inner leaflet, respectively, and a_0 is the average equilibrium cross-section area of one membrane molecule. On the other hand, the vesicle has a geometrical area difference given by $\Delta A = A^+ - A^- = 2d \oint \mathrm{d}AH$, where A^+ and A^- are surface areas of the membrane in the outer and inner leaflet, respectively, d is the distance between the neutral surfaces of the two leaflets,[146] *i.e.*, roughly half the bilayer thickness, see Fig. 2b, and $H = (C_1 + C_2)/2$ is the mean curvature. A neutral surface is defined by the property that bending and stretching are decoupled in energy when both deformations are defined with respect to it. If N^+ and N^- can be regarded as constant during vesicle deformation, the difference between ΔA_0 and ΔA will be compensated by the expansion or compression of the cross-section area of the membrane molecules. This elastic energy that is associated with the deformation of the membrane is called the "area difference elastic energy" and is expressed by $w_{\text{ADE}} = (\kappa_{\text{r}}/2Ad^2)(\Delta A - \Delta A_0)^2$ (κ_{r} is the nonlocal bending rigidity[147]). The ADE model[126–128] is expressed by the sum of the bending energy and the area difference elastic energy

$$F_{\text{ADE}} = \frac{\kappa}{2}\oint \mathrm{d}A(C_1 + C_2)^2 + (\kappa_{\text{r}}/2Ad^2)(\Delta A - \Delta A_0)^2 + \kappa_{\text{G}} \oint \mathrm{d}AC_1C_2, \quad (2)$$

where the ADE model deals with a symmetric bilayer. For asymmetric membranes, the ADE model is modified by taking into account spontaneous curvature:[129]

$$F_{\text{ADE+SC}} = \frac{\kappa}{2}\oint \mathrm{d}A(C_1 + C_2 - C_0)^2 + (\kappa_{\text{r}}/2Ad^2)(\Delta A - \Delta A_0)^2 + \kappa_{\text{G}} \oint \mathrm{d}AC_1C_2. \quad (3)$$

This ADE model including spontaneous curvature is equivalent to the ADE model without considering spontaneous curvature using the renormalized area-difference ΔA_0, given by $\Delta\tilde{A}_0 = \Delta A_0 + 4\pi\kappa d C_0 R_0^2/\kappa_{\text{r}}$.[148]

For (single chain) fatty acid vesicles that are considered[11,149,150] as potentially prebiotic compartment systems, a transient difference between ΔA_0 and ΔA rapidly relaxes[151–153] due to fast fatty acid flip-flop motions (~milliseconds).[29,154] Thus, the deformation of fatty acid vesicles is well described by the "spontaneous curvature model" ($\Delta A_0 = \Delta A$). In contrast, for phospholipid bilayers, the time scale for flip-flop motions (~several hours)[155,156] is much longer if compared to the vesicle deformation time scale (~several seconds), although the flip-flop rate depends on the mechanical shear stress between inner and outer leaflet.[157] Based on experimental data, the deformation of (double chain) phospholipid vesicles is well described by the ADE model, indicating that the flip-flop motion during the deformation is negligible.[135,136]

To attain vesicle division, the spherical vesicle has to deform to the limiting shape vesicle (Fig. 2a), and then the membrane neck of the limiting shape vesicle, *i.e.*, the lipidic connection between the two vesicles, needs to be broken (destabilized). According to the spontaneous curvature model, the dependence of the bending energy of a pear vesicle (Fig. 2d) on the neck size is given by

$$F_{\text{A,V}}(a_{\text{ne}}) - F_{\text{A,V}}(0) \approx 4\pi a_{\text{ne}}\kappa\left[C_0 - \left(\frac{1}{R_1} + \frac{1}{R_2}\right)\right], \quad (4)$$

where the pear vesicle (area A and volume V) is expressed by two spheres with radii R_1 and R_2 ($R_1 \neq R_2$) connected by a narrow neck with radius a_{ne}, and $a_{\text{ne}} = 0$ for the limiting shape vesicle.[131,158,159] For $\left(\frac{1}{R_1} + \frac{1}{R_2}\right) > C_0$, the neck with a finite size becomes stable, whereas for $\left(\frac{1}{R_1} + \frac{1}{R_2}\right) < C_0$, the lowest energy state is the one with neck size $a_{\text{ne}} = 0$, *i.e.*, the conditions for a destabilization of the neck. In other words, if the spontaneous curvature C_0 is larger than $\left(\frac{1}{R_1} + \frac{1}{R_2}\right)$, breaking of the neck is expected to occur. To compare the elastic energy between the one-vesicle state (before division) and a two-vesicle state (after division), the Gaussian bending energy term plays an important role.

The free energy landscape from a pear vesicle with a neck radius a_{ne}, (state "1") to a two-"daughter vesicles" state with radii R_1 and R_2 ($a_{\text{ne}} \ll R_1, R_2$) (state "2") through a breaking of the limiting shape neck (state "b") is schematically shown in Fig. 3.[160] Assuming that the bending energy of the limiting shape is equal to that of the two vesicle state, the free energy difference between state "1" and state "2" is expressed by

$$F_{\text{SC,2}} - F_{\text{SC,1}} \cong -4\pi a_{\text{ne}}\kappa\left[C_0 - \left(\frac{1}{R_1} + \frac{1}{R_2}\right)\right] + 4\pi\kappa_{\text{G}} = \Delta_{21}. \quad (5)$$

For $|C_0| \ll \left(\frac{1}{R_1} + \frac{1}{R_2}\right)$, the free energy difference is $\Delta_{21} \approx 4\pi\left(a_{\text{ne}}\left(\frac{1}{R_1} + \frac{1}{R_2}\right)\kappa + \kappa_{\text{G}}\right)$, whereas for $C_0 \approx \frac{1}{a_{\text{ne}}} \gg \left(\frac{1}{R_1} + \frac{1}{R_2}\right)$, $\Delta_{21} \approx -4\pi(\kappa - \kappa_{\text{G}})$. Thus, the Gaussian bending energy term governs the vesicle division. Although the estimation of the Gaussian bending rigidity, κ_{G}, is still controversial,[161–165] it is sufficient to use the rough estimate $\kappa_{\text{G}} \simeq -\kappa$. In this case, when the membrane has a small spontaneous curvature,

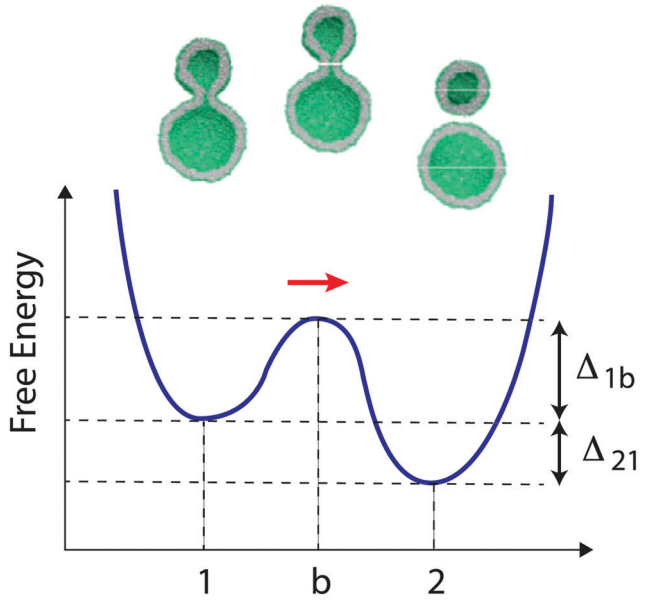

Fig. 3 Schematic free energy diagram for the vesicle division process, with the free energy barrier indicated for breaking the neck of the limiting shape vesicle (Δ_{1b}). For the division process to be "downhill" (exergonic) in free energy, the free energy difference Δ_{21} between the two-vesicle state 2 and the pear state 1 must be negative. The velocity or rate of the fission process, on the other hand, is determined by the positive free energy barrier Δ_{1b}. (This figure is taken from R. Lipowsky, *Adv. Biol.*, 2021, 2101020; open access article.)

$\Delta_{21} \approx -4\pi\kappa < 0$, and when the membrane has a large spontaneous curvature, $\Delta_{21} \approx -8\pi\kappa < 0$. Therefore, the vesicle division is preferable if the vesicle overcomes the free energy barrier Δ_{1b} governed by the spontaneous curvature, eqn (4), and the local disruption of the bilayer structure. Experimentally, the division of the limiting shape vesicle into two vesicles is a very rare event because the narrow neck connecting two spherical vesicles in the limiting shape vesicle is quite stable.[166] Several means have been proposed to overcome the energy barrier as shown in Section 2.5.

2.3. Vesicle membrane growth

For sustainable vesicle reproduction, the vesicle membrane area must be increased by incorporating membrane molecules. There are three main approaches to achieve vesicle membrane growth:[167] (1) incorporation of membrane molecules from the external bulk solution into the vesicle membrane, (2) synthesis of membrane molecules within the vesicle, and (3) fusion with other vesicles. In the following, we will provide examples of studies on membrane growth by each of these three approaches.

2.3.1. Incorporation of membrane molecules from external solution. According to Fick's law, the flux of membrane molecules from the external solution into the vesicle membrane (area A) can be expressed by[168]

$$\frac{\partial A}{\partial t} = A\frac{N_A a_0 c D}{l_D k_B T}(\mu_{ext} - \mu_{mem}), \quad (6)$$

where N_A is the Avogadro number, a_0 is the average equilibrium cross-section area of a membrane molecule, c is the concentration of membrane molecule in the external solution, D is the diffusion coefficient of the membrane molecule, l_D is a characteristic length scale relevant to the membrane molecule transport in the vicinity of the vesicle surface ($\sim$2 μm for fatty acids), k_B is the Boltzmann constant, and T is the temperature. The driving force, $\Delta\mu = \mu_{ext} - \mu_{mem}$, is the chemical potential difference between the membrane molecule in the external solution (μ_{ext}) and the membrane molecule in the vesicle membrane (μ_{mem}). At equilibrium state, both chemical potentials have the same value, *i.e.*, there is no net flux of membrane molecules. In order to drive vesicle growth, one possible way is to increase μ_{ext} by reducing the hydrophilicity of the membrane molecules to be incorporated. In the case of fatty acids, which probably were among the first amphiphilic molecules on the primitive Earth,[11,149] vesicle growth can be triggered by controlling the degree of dissociation of the carboxylic acid group.[150,169] At low pH, the carboxylic acid is in its undissociated neutral form, which results in the formation of an oil phase (if the fatty acid is kept above its melting temperature), whereas at high pH values, the molecules are deprotonated and therefore negatively charged (ionized), resulting in the formation of micelles or vesicles (if the concentration is above the critical aggregation concentration, cac). The formation of fatty acid vesicles is restricted to a rather narrow pH range (*ca.* 7–9), where approximately half of the carboxylic acid groups are ionized. Although the pK_a of a non-associated carboxylic acid monomer is typically 4–5,[170] a fatty acid molecule embedded within a bilayer membrane has an apparent pK_a of 7–9 due to the condensation of counter ions on the membrane surface.[171] Accordingly, the cac depends on the pH value of the bulk solution, for example, the cac of decanoic acid/decanoate varies from 14 mM at pH = 6.8 (decanoic acid + decanoate vesicles) to about 100 mM at pH = 11.8 (decanoate micelles).[169] Therefore, when a fatty acid solution with a high pH (the dominating form of the fatty acids clearly being the deprotonated species) is added to a dispersion of fatty acid vesicles with a pH around the pK_a of the membrane-embedded fatty acid molecules, the pH drop encourages protonation of the ionized fatty acids originally present in the high pH solution and reduces the fatty acids' hydrophilicity, which results in a flux of fatty acid molecules toward the vesicles, *i.e.*, the vesicle membrane grows.[169,172,173]

In the case of micrometre-sized ("giant") vesicles formed from oleic acid and oleate molecules, vesicle membrane growth was visualised by confocal microscopy, see Fig. 4.[173] Added fatty acid molecules first encountered the outermost leaflet and then moved to the inner leaflet(s) by fast flip-flop motions of the neutral form (oleic acid). On the other hand, the volume of the vesicle could not increase within the time-scale of the membrane area growth. For the multilamellar vesicle shown in Fig. 4A, the outermost membrane grew faster than the inner membrane layers and formed protrusions (B, C), while for the unilamellar spherical vesicle (F), deformation into a prolate shape vesicle occurred (G). Based on the time evolution of the light scattering intensity of submicrometre-sized oleic acid/oleate vesicles, two pathways appear to exist for the incorporation of oleate micelles into the vesicles: one is the adsorption of

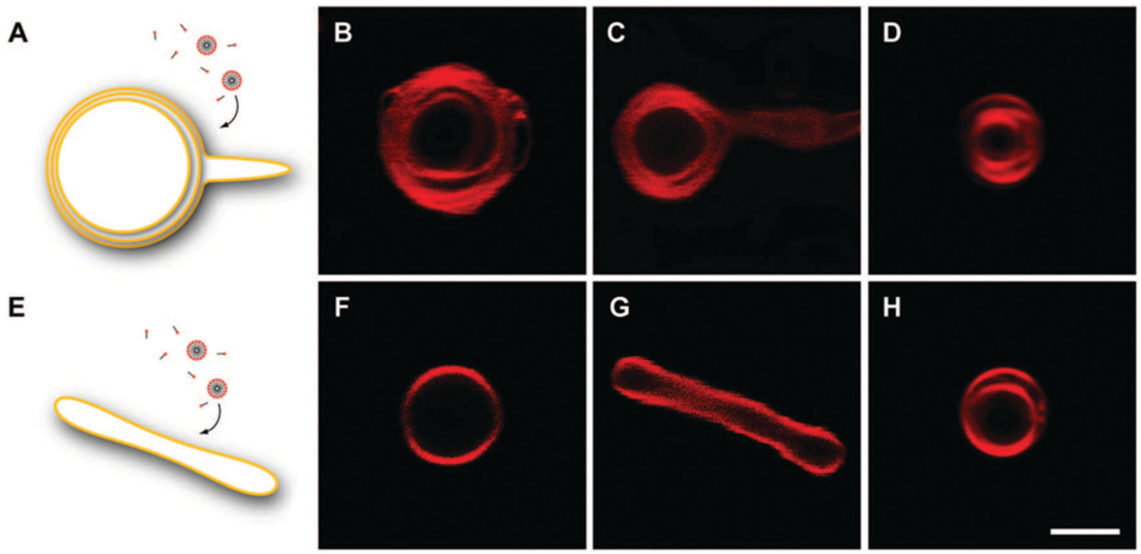

Fig. 4 (A) Schematic diagram of the incorporation of oleate micelles into a multilamellar oleic acid/oleate vesicle: the outermost membrane grows faster than the inner membrane layers. (B and C) Confocal images of a multilamellar oleic acid/oleate vesicle (containing 0.2 mol% red fluorescent 1,2-dihexadecanoyl-*sn*-glycero-3-phosphoethanolamine-rhodamine, Rh-DHPE) at pH 8.5, before and 10 min after the addition of oleate micelles, respectively. (D) Confocal image of a multilamellar vesicle after division by mild shear. (E) Schematic drawing of the incorporation of micelles into a unilamellar vesicle. (F and G) Confocal images of a unilamellar oleic acid/oleate vesicle before and 10 min after the addition of oleate micelles, respectively. (H) Confocal image of a multilamellar vesicle formed after the agitation of elongated unilamellar vesicles. Scale bar for (B–D) and (F–H): 2 μm. (Reprinted with permission from T. F. Zhu and J. W. Szostak, *J. Am. Chem. Soc.*, 2009, **131**, 5705–5713. Copyright 2009 American Chemical Society.) https://pubs.acs.org/doi/full/10.1021/ja900919c.

micelles on the vesicle surface followed by incorporation into the vesicles, and the other is the formation of unstable intermediate aggregates formed from micelles before adsorption and incorporation into the vesicles.[172] A similar vesicle growth is also driven by concentration changes, whereby at low concentration, fatty acids prefer to form small micellar aggregates, whereas at high concentration large vesicle aggregates are formed preferentially.[174]

Vesicle growth induced by a modification of the chemical potential of the membrane molecules was observed in other systems: (i) the clay mineral montmorillonite was shown to facilitate the spontaneous conversion of fatty acid micelles into fatty acid vesicles. When clay particles were encapsulated inside – or associated with – fatty acid vesicles, the vesicles showed accelerated uptake of fatty acid molecules supplied as micelles and showed vesicle growth, which suggests the possible role of mineral particles for vesicular protocell formation at the origin of life.[175] Please note the inconsistency in the terminology used. Although ''fatty acid micelles'' mainly consist of soap molecules (the deprotonated form of the fatty acids), the term ''fatty acid micelle'' is often used instead of the more appropriate ''soap micelles''. Similarly, the term ''fatty acid vesicles'' is frequently used, although ''fatty acid/soap vesicles'' would be more appropriate, because the membrane boundary consists of two chemically different species, a fatty acid and its corresponding soap. (ii) When the hydrophobic dipeptide *N*-acetyl-L-phenylalanine leucinamide ($AcPheLeuNH_2$) was embedded in fatty acid vesicle membranes, this dipeptide promoted the incorporation of fatty acid micelles into the vesicle membrane, which accelerated the growth of the vesicles.[12] (iii) The third example for demonstrating vesicle membrane growth through incorporation of membrane-forming molecules is completely different from fatty acid vesicles and is not an example of a prebiotically plausible case. This example, however, serves to illustrate how vesicle growth can be achieved by regulating the chemical potential of membrane molecules to promote their membrane incorporation. This vesicle system consists of anionic AOT [sodium bis-(2-ethylhexyl)sulfosuccinate] vesicles and enzymatically *in situ* formed polyaniline in its emeraldine salt form (PANI-ES). PANI-ES can form hydrogen bonds with ionized AOT molecules, which reduces the hydrophilicity of the AOT molecules present in the external solution, resulting in incorporation of AOT molecules and with this promoting AOT vesicle growth.[176] Therefore, vesicle growth is encouraged by a regulation of the chemical potential of the membrane molecules present in the external solution through interactions with specific molecules (PANI-ES).

2.3.2. Vesicle growth coupled with the synthesis of membrane molecules. Membrane growth coupled with the synthesis of membrane molecules is experimentally very challenging. The examples given are not prebiotically plausible or biological. They might, however, help to understand the chemical and physical requirements for a vesicular protocell or a ''minimal cell'' system to undergo vesicle growth due to membrane molecule synthesis. In the first experiments of vesicle growth coupled to the synthesis of bilayer-forming membrane molecules, oleic acid molecules were obtained by hydrolysis of oleic anhydride.[177,178] The experiments were carried out by adding a drop of oleic anhydride on top of an aqueous oleic acid vesicle dispersion at pH = 8.5. Hydrolysis of anhydride molecules at the water–anhydride droplet interface

and of those anhydride molecules that partitioned into the hydrophobic area of the oleic acid vesicle membrane yielded new oleic acid and oleate molecules, which resulted in vesicle membrane growth. In the latter case, the anhydride hydrolysis took place locally in the area of the vesicle membrane. Two types of vesicle transformations were observed: one was along a budding pathway where the mother vesicle deformed to a pear-like shape and then divided into two vesicles, and another one is called "vesicle birthing",[179] where a mother vesicle containing an internal vesicle – which was accidentally trapped during the vesicle formation process – expelled the trapped vesicle from the mother vesicle (Fig. 5-I).

A well-designed chemical system for the synthesis of membrane molecules within the vesicle membrane is the one proposed by Sugawara's group.[180–183] It is based on the design of a non-natural membrane-forming amphiphile, abbreviated as V, and its precursor molecule V* (Fig. 5-IIa). V* is a bola-amphiphile containing two polar headgroups that are connected *via* a hydrophobic linker containing an imine bond. Hydrolysis of this bond yields V and an electrolyte E through the aid of a catalyst C. When the precursor V* is added to a suspension of giant vesicles composed of the membrane molecule V and catalyst C, V* is hydrolysed within the vesicular membrane embedding C. The mother vesicle showed growth and division due to the produced membrane molecules V as shown in Fig. 5-IIb.

More recently, the Devaraj's group developed various systems for synthesising membrane molecules ("anabolism type") that mimic the phospholipid synthesis process of contemporary cellular life, where phospholipids with two hydrophobic tails are synthesised by combining lysophosphatidic acids (LPA) and an acyl donor (see Fig. 1b).[49,184] In the first example (Fig. 6a),[185] the phospholipids were synthesised by combining an alkyl azide and an alkyne lysolipid within the membrane with the aid of a copper catalyst, whereby the copper catalyst was also synthesised within the membrane (A–C). The lipid synthesis caused the growth of pre-existing vesicles (D). The second example is the realisation of the growth of vesicles without pre-existing vesicles, *i.e.*, a *de novo* vesicle formation.[186,187] Fig. 6b shows the reaction of lysophosphatidylcholine (LPC) with the acyl donor sodium 2-(oleoylthio) ethane-1-sulfonate in water for the synthesis of a phospholipid without enzymes[188] (A–C). In this example, at the initial state, no vesicles could be detected; however, after 10 min tubular vesicles appeared, after 30 min spherical vesicles, and finally various types of vesicles were formed after 60 min (D). The third example is a synthetic mimic of the phospholipid biosynthesis process occurring inside biological cells (Fig. 6c). As shown in (A), the highly reactive intermediate dodecanoyl-AMP (1) was synthesised by reacting dodecanoic acid (DDA) with ATP in the presence of the enzyme FadD10. Dodecanoyl-AMP (1) reacted with amine-functionalized lysolipids (2) to obtain phospholipids (3), resulting in spontaneous vesicle growth (B).[189] In addition, Devaraj's group also succeeded in synthesising phospholipids using the enzyme, fatty acyl CoA ligase (FACL).[190] Similar membrane growth using an "anabolism type" of reaction scheme was reported by Toyota's group.[191] All these examples are highly challenging approaches that try to realize membrane growth systems that mimic contemporary cellular life systems.

2.3.3. Vesicle growth by fusion of vesicles. Another way to grow membranes is through vesicle fusion.[192] The fusion of vesicles is an effective means to supply membrane molecules and ingredients to target vesicles. The fusion process of two bilayers can be described as follows:[193–196] When two bilayers come close to each other and make a physical contact, the formed contact area grows. Then, inter-bilayer flips of the bilayer-forming molecules take place and lead to the formation of a disordered membrane domain. In this disordered region, lipids reorder to form a hemifused state (with a contact area that consists of a common bilayer)[197] and finally form a fusion pore (an opening which allows the exchange of the internal aqueous solutions). Membrane fusion is completed after expanding this fusion pore (through inflation). Overall, for vesicle fusion to occur, the vesicles that fuse first must come in contact, *i.e.*, they must adhere to each other. However, since the surface of the vesicles is strongly hydrated and the vesicle surface carries charges in most cases including neutral phospholipid vesicles,[198–200] adhesion of the same type of vesicles is prevented due to electrostatic repulsions between the vesicles. Consequently, one approach for fusing vesicles is to utilize electrostatic attractions between cationic and anionic vesicles.[201–204] Fig. 7 shows morphological transformations involving a negatively charged giant unilamellar vesicle (GUV) composed of POPC (1-palmitoyl-2-oleoyl-*sn-glycero*-3-phosphocholine) and POPG [1-palmitoyl-2-oleoyl-*sn-glycero*-3-phospho-(1′-*rac-glycero*l)] (and labelled by using small amounts of NBD-PE, 1,2-dipalmitoyl-*sn-glycero*-3-phosphoethanolamine-*N*-(7-nitro-2-1,3-benzoxadiazol-4-yl), a green fluorescent lipid). Morphological transformations were induced by addition of positively charged large unilamellar vesicles (LUVs) composed of DOTAP (1,2-dioleoyl-3-trimethylammonium-propane), DOPE (1,2-dioleoyl-*sn-glycero*-3-phosphoethanolamine), and a red fluorescent lipid (DPPE-rhodamine).[204] The initially green GUV changed to red with elapse of time due to fusion with red LUVs, and at the same time, the shape of the green GUV became flabby due to an increase in membrane area (Fig. 7A). The fusion of a single LUV (red) with a GUV (green) is visualized in Fig. 7B. The LUV attached to the GUV (red spot indicated by an arrow), followed by fusion and diffusion of the red fluorescent dye into the GUV membrane on a timescale of 1–2 seconds.

The vesicle fusion method just described cannot be used to fuse vesicles having the same membrane composition. In order to fuse vesicles having the same membrane composition, a strong adhesion force is required to overcome repulsive electrostatic interactions or to overcome hydration forces. This can be achieved by adding membrane fusion-promoting molecules. For example, to mimic membrane fusion induced by proteins such as SNARE, a DNA template strand and its complementary strand of DNA were anchored to the surface of vesicles present in two separately prepared vesicle dispersions; hybridization of the complementary DNA strands reduced the inter-vesicle distance, resulting in vesicle hemifusion and finally fusion.[205,206] In another example, amphiphilic ligands with a β-diketone

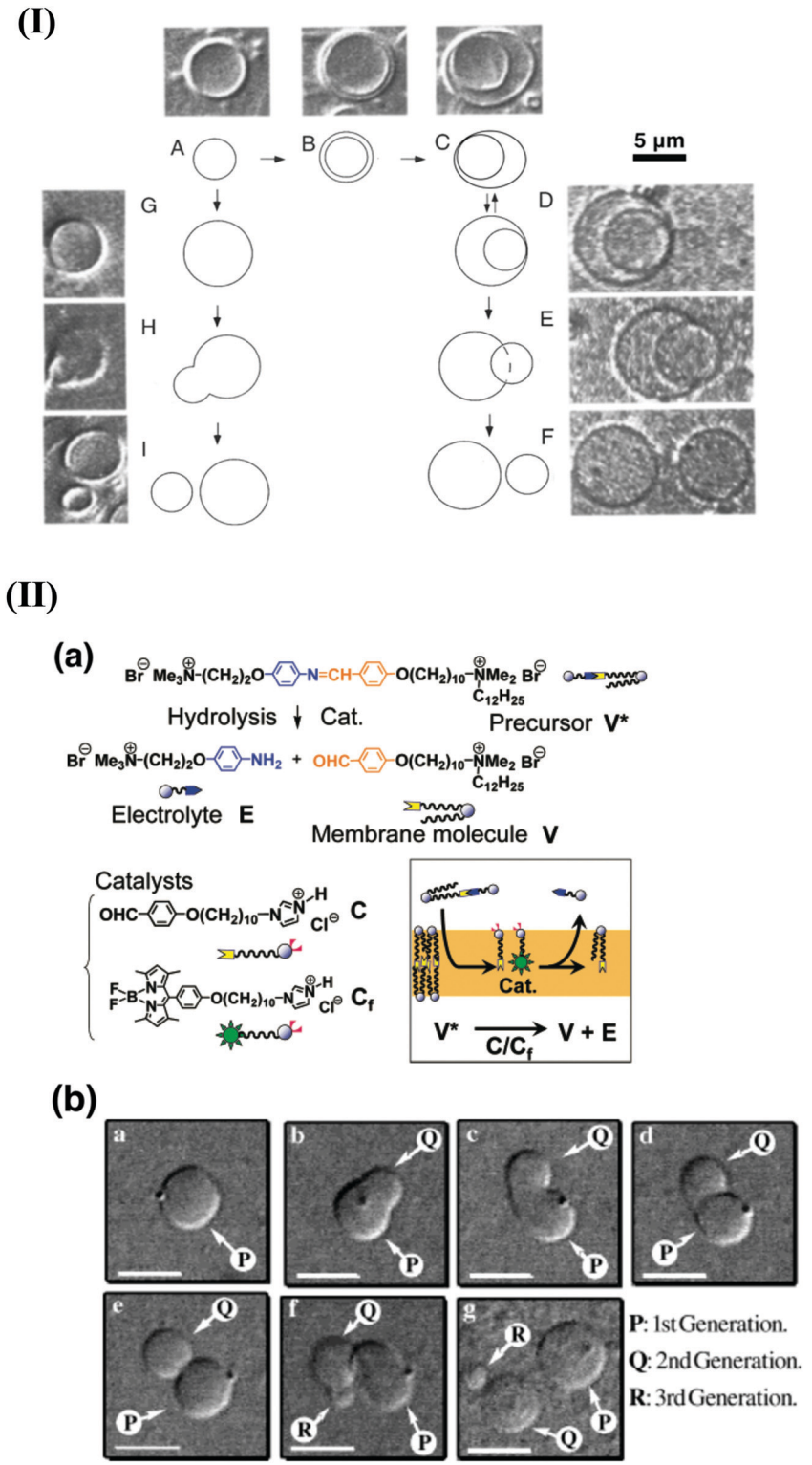

Fig. 5 Vesicle growth and division coupled with the synthesis of membrane molecules. (I) Growth and division of oleic acid/oleate giant vesicles coupled with the hydrolysis of oleic anhydride. Oleic acid/oleate giant vesicle transformations and two self-reproduction processes following intralamellar oleic anhydride hydrolysis at pH = 8.5. (A–C) Formation of "inclusion vesicles" (picture B was taken 2 h after A; C was taken 8 h after B). (D–F) Vesicle "birthing" (picture E was taken 5 s after D: F was taken 2 s after E). (G–I) Vesicle budding (picture H was taken 10 s after G: I was taken 5 s after H). The scale bar represents 5 μm for all micrographs. (Reprinted with permission from R. Wick *et al.*, *J. Am. Chem. Soc.*, 1995, **117**, 1435–1436. Copyright 1995 American Chemical Society.) (II) A well-designed chemical system for vesicle reproduction coupled with the hydrolysis of membrane precursor molecules. (a) Chemical scheme of the self-reproduction of giant multilamellar vesicles (GMVs). The membrane molecule V and electrolyte E are formed by the hydrolysis of the membrane precursor V* in the presence of the catalyst C and the fluorescence probe C_f, which are anchored within the vesicular membrane (panel at the bottom right). (Reprinted with permission from T. Toyota *et al.*, *Langmuir*, 2008, **24**, 3037–3044. Copyright 2008 American Chemical Society.) (b) Morphological changes in a GMV composed of V and C: (a–g) images obtained at different times after mixing of a dispersion of GMV and a solution of precursor V*. Scale bar: 10 μm. (Reprinted with permission from K. Takakura *et al.*, *Langmuir*, 2004, **20**, 3832–3834. Copyright 2004 American Chemical Society.)

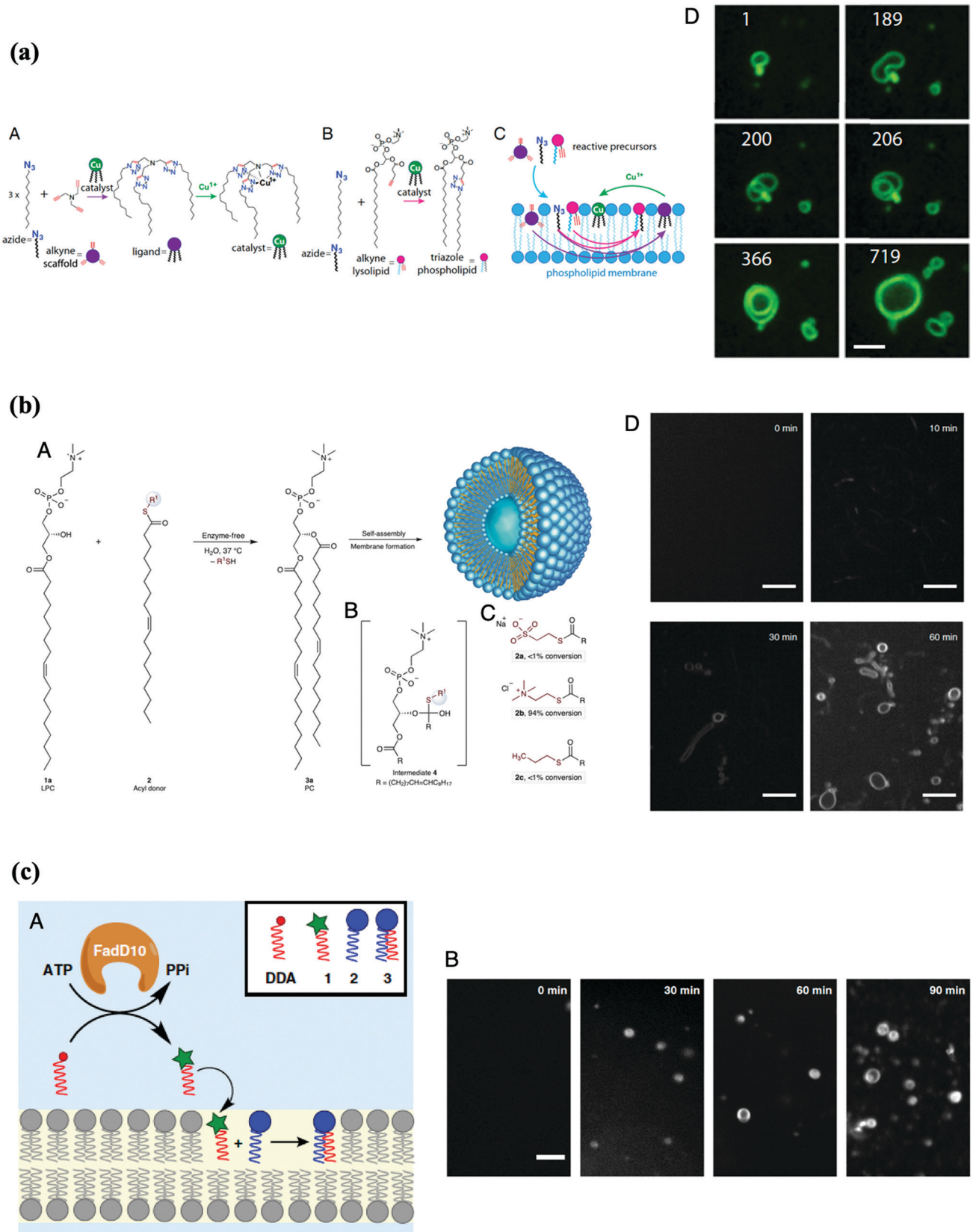

Fig. 6 Vesicle growth induced on the basis of non-biological chemical syntheses of phospholipids. (a) Triazole phospholipid synthesis driven by a self-reproducing catalyst and by membrane growth. (A) The ligand tris-(lauryl triazole)amine (TLTA) was synthesized by combining a tripropargylamine scaffold with 1-azidododecane, TLTA is capable of binding Cu^{1+} ions to form a catalytically active complex (catalyst). This copper complex catalyses the synthesis of a new ligand from 1-azidododecane (azide) and tripropargylamine (alkyne scaffold), which, upon metallation, produces additional catalytic molecules. (B) The copper complex also catalyses the formation of a triazole phospholipid from 1-azidododecane (azide) and an alkyne modified lysolipid. (C) Membrane-embedded catalysts act on azide and alkyne reactive precursors, synthesizing additional phospholipid and oligotriazole ligands. (D) Lipid synthesis-mediated growth results in an increase in membrane surface area and volume. The shape change depicted here results in the formation of a multilamellar vesicle at 206 min. Numbers indicate elapsed time, in minutes, from the start of imaging. Scale bar, 3 μm. (Reprinted with permission from M. D. Hardy *et al.*, *Proc. Natl. Acad. Sci. U. S. A.*, 2015, **112**, 8187, Copyright 2015 National Academy of Sciences. (b) Enzyme-free synthesis of natural phospholipids. (A) *De novo* synthesis of a diacylphospholipid (PC, **3a**) from lysophosphatidylcholine (LPC, **1a**) and a thioester as acyl donor (**2**) in water leading to an *in situ* self-assembled membrane (a PC vesicle). The leaving group is shown in red. (B) Chemical structure of the proposed reaction intermediate (**4**). (C) Structures of the reactive fatty acyl derivatives R used (red part in **2** and **4**). (D) Fluorescence micrographs of the enzyme-free formation of phospholipid membranes. Scale bars, 10 μm. (Reprinted with permission from L. Liu *et al.*, *Nat. Chem.*, 2020, **12**, 1029–1034, Copyright 2011 Springer Nature.) (c) *De novo* formation of phospholipid membranes based on adenylate chemistry. (A) A phospholipid synthetic pathway, where first reactive lipid precursors [DDA, dodecanoic acid] are converted to dodecanoyl-AMP (**1**) through enzyme FadD10, and then chemoselective reaction of (**1**) and amine-functionalized lysolipids (**2**) produces phospholipids (**3**). (B) Time series of confocal microscopy images of *de novo* phospholipid (**3**) vesicle formation resulting from the incubation of an aqueous solution of DDA, lysolipid (**2**), ATP, FadD10 at 37 °C. Scale bar: 10 μm. (This figure is taken from A. Bhattacharya *et al.*, *Nat. Commun.*, 2019, **10**, 300; open access article.)

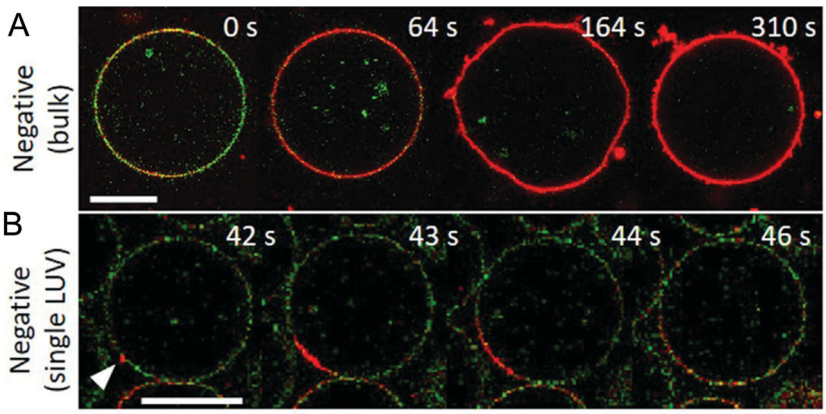

Fig. 7 Morphological transformations of negatively charged POPC/POPG (1 : 1) GUVs upon addition of positively charged DOTAP/DOPE (1 : 1) LUVs. (A) The negatively charged GUV initially shows green fluorescence due to the presence of DPPE-NBD and quickly acquires a strong red fluorescence from positively charged LUVs containing DPPE-Rh (64 s). Further arrival of LUVs increases the vesicle fluctuation, indicating area gained by fusion (164 s). (B) A single LUV fusion event. The arrowhead at 42 s points to the initially docked LUV. The single fusion events are characterized by a local increase in fluorescence resulting from initial lipid dilution (self-quenching is lost), followed by a decrease in fluorescence as the LUV lipids diffuse away from the fusion point and get diluted into the GUV membrane. Scale bars: 20 μm. (Reprinted with permission from R. B. Lira *et al.*, *Biophys. J.* 2019, **116**, 79–91. Copyright 2019 Biophysical Society.)

head group that can be cross-linked by Eu^{3+} ions were used. Two GUVs embedded with the ligands were brought into close contact with each other using micropipettes, and Eu^{3+} ions were added to drive vesicle fusion.[207]

For successful vesicle fusion, the required inter-bilayer flip of the membrane molecules in the expanded contact area is a barrier to overcome (see above). The question then is how to overcome this barrier. According to simulation studies, membrane tension is a key to induce inter-bilayer flip of membrane molecules.[195,208] There are two ways to increase membrane tension; either by decreasing the vesicle membrane area or by increasing the vesicle volume.

In the first case, for fatty acid vesicle systems, the tension of the membrane can be increased by increasing the pH of the vesicle dispersion. This results in a release of the ionized form of the fatty acid from the vesicles into the external solution due to an increase in cac (higher water solubility of the deprotonated form of the fatty acid). This migration of fatty acid molecules from the vesicle membrane into the bulk solution increases the membrane tension, which results in vesicle fusion.[209] Modulation of the cross-section area of a lipid by ion binding is another possibility to decrease the membrane area.[210,211] Most metal ions bind to the head groups of bilayer-forming phospholipids and produce more ordered bilayers than in the absence of the metal ions, resulting in a smaller area per lipid molecule as compared to a metal ion-free system. The membrane tension that is induced by ion binding most likely is responsible for the observed La^{3+} ion-induced fusion of vesicles consisting of two lipids, DOPC and DPOPE (1,2-dioleoyl-*sn-glycero*-3-phosphocholine and 1,2-dipalmitoleoyl-*sn-glycero*-3-phosphoethanolamine).[212]

For the second case (increase in vesicle volume), an osmotic pressure difference between the inside and the outside of the vesicles is implemented to promote the flow of water molecules from the bulk solution into the aqueous interior of the vesicles.

This can be achieved, for example, by encapsulating dextran inside lipid GUVs consisting of oleic acid and POPC (at a molar ratio of 1 : 1), or of DOPC : DOPE : 1-hydroxy-2-oleoyl-*sn-glycero*-3-phosphocholine (70 : 15 : 15, mol ratio). When SUVs (small unilamellar vesicles) with the same membrane composition were added to the swollen GUV suspension, the SUV fused with the GUVs to reduce the membrane tension, resulting in vesicle growth.[213]

2.4. Deformation of a spherical vesicle to a limiting shape vesicle

The phase diagram reflecting the spontaneous curvature model (Fig. 2c) shows that spherical vesicles do not deform to an (outward) limiting shape by only increasing the membrane area (decrease of reduced volume). For a symmetric spherical bilayer (reduced spontaneous curvature $c_0 = 0$), an increase of the membrane area at constant volume will cause a series of vesicle deformations, sphere → prolate → oblate (green dotted arrow in Fig. 2c), but there will be no deformation to a limiting shape. In order to transform a spherical vesicle into a limiting shape vesicle (*e.g.*, light blue arrow in Fig. 2c), a reduced spontaneous curvature c_0 that reaches the L^{pear} line is required. There are two ways to impose the necessary spontaneous curvature to the bilayer: (i) by adding "asymmetrically shaped" membrane molecules, *i.e.*, membrane molecules that do not have a cylindrical shape for optimal packing into a flat bilayer,[214] or (ii) by anchoring macromolecules to the outer leaflet of the bilayer.[159,215]

Generally, membrane molecules that form vesicles have an almost cylindrical ("symmetrical") shape when present in an aggregated state in a water-rich medium.[216] When cone-shaped ("asymmetrical") amphiphiles (here referring to molecules with a large polar head group and small hydrophobic tails, which results in a positive molecular spontaneous curvature) are added to a spherical vesicle, these cone-shaped molecules tend to localize in the outer leaflet due to molecular shape preference.[217] In the case of the addition of inverse cone-shaped amphiphiles (molecules with a small polar head group and large hydrophobic tails, which results in a negative molecular spontaneous curvature), they tend to localize in the inner leaflet.[218] The coupling between molecular shape and membrane mean curvature plays an important role in some of the biological functions of cell membranes.[219–222] When asymmetrically shaped amphiphiles are added to a vesicle bilayer composed of cylinder-shaped amphiphiles, the spontaneous curvature of the binary membrane is expressed by $C_0 = \frac{1}{2}C_a(\phi_a^+ - \phi_a^-) = \frac{1}{2}C_a\Delta\phi_a$, where C_a is the molecular spontaneous curvature of the asymmetrically shaped amphiphile and ϕ_a^+ and ϕ_a^- are the area fraction of the asymmetrically shaped amphiphile in the outer and inner leaflet, respectively.[223] For example, cholesterol and phosphatidylethanolamine (PE) are known as inverse cone-shaped amphiphiles with negative spontaneous curvature, *e.g.*, for PE lipids $C_a \cong -0.3\ nm^{-1}$,[224] which encourages vesicles to reach an outward limiting shape.[176,223] Here we consider a binary vesicle composed of AOT (a cylinder shape amphiphile if excess counterions are present in aqueous solution) and cholesterol with fast flip-flop rates.[154,225] At the equilibrium state, the concentration difference, $\Delta\phi_a$, obtained by minimization of the total energy composed of the elastic energy and the mixing free energy,[226,227] is very small (*e.g.*, $\Delta\phi_a \sim -10^{-5}$ for a binary AOT/cholesterol vesicle with $R = 10\ \mu m$), resulting in a reduced spontaneous curvature of $c_0 = C_0R_0 \sim 0$. When AOT molecules in the external solution are incorporated into the outer leaflet of the vesicle bilayer and then move to the inner leaflet by flip-flop motions, the concentration of cholesterol in the outer leaflet is determined by a balance of uptake rate and flip-flop rate. If the AOT uptake rate is faster than the AOT flip-flop rate, the AOT concentration difference $\Delta\phi_a$ is enhanced and simultaneously, the vesicle size $R_0 = (A/4\pi)^{1/2}$ is increased. Due to both contributions, enhanced membrane composition asymmetry and vesicle size increase, the binary vesicle deforms to the limiting shape vesicle, *i.e.*, c_0 reaches the L^{pear} line (Fig. 2c). On the other hand, AOT vesicles without cholesterol grow to a tubular shape rather than to the limiting shape when AOT molecules are supplied. Thus, an inverse cone-shaped amphiphile plays a key role to attain vesicle division.[176]

As mentioned above, spontaneous membrane curvature can also be generated in GUVs by anchoring macromolecules (*e.g.* proteins) to the outer leaflet of the vesicle bilayer. Steinkühler *et al.* found a linear relationship between spontaneous curvature and coverage of the GUV surface by anchored GFP (green fluorescent protein), showing GUV deformation to limiting shape vesicles.[159]

Another way to deform a spherical vesicle into a limiting shape vesicle is to use depletion interactions of particles encapsulated in the vesicle.[228–231] The depletion interaction[232,233] was originally observed for binary mixture suspensions composed of large hard colloids and small polymer coils (see, for example, Fig. 1 in ref. 234). Each colloidal particle is surrounded by a depletion zone that is the region next to each colloid surface, which is inaccessible to the centres of the polymer coils. If the depletion zones of two colloids overlap, the free volume for the polymer coils increases, which raises the translational entropy of the polymer coils, but at the expense of lowering the entropy of mixing. At high polymer concentration, the translational entropy dominates the system, and the colloidal particles aggregate to minimize the depletion zone. When particles are confined inside a vesicle, the inner surface of the vesicle membrane will have a depletion zone. In order to maximize the translational entropy of the confined particles, this depletion zone needs to be minimized. In the range of $0.7 < \nu < 0.9$ (ν being the reduced volume), the translational entropy can be maximized by deforming a prolate, oblate, or stomatocyte vesicle into a limiting shape vesicle.[228] Such deformation of vesicles into limiting shape vesicles due to depletion interactions was observed by confining colloidal particles[228] and polymers[229] inside vesicles.

2.5. Division of vesicles

To realize the reproduction of vesicles, it is necessary to break the membrane neck of the limiting shape vesicle. Various studies were devoted to the question of how to break the neck.[235] As explained in Section "2.2. Membrane elasticity model of vesicle reproduction", it is difficult to destabilize the neck in a single-component vesicle. Therefore, divisions usually are achieved in multicomponent lipid vesicles.[166,214] According to the membrane

elasticity model, a straightforward method for destabilizing the neck is to introduce a large spontaneous curvature.[160] The waistline (wl) of the neck in pear-shaped vesicle forms a circle with radius a_{ne} (see Fig. 2d). Along this waistline, the neck is characterized by two principal curvatures, the negative principal curvature $C_{1,wl} < 0$ perpendicular to the waistline and the positive principal curvature $C_{2,wl} = 1/a_{ne} > 0$ parallel to the waistline. When the neck closes, the neck radius goes to zero (limiting shape) and the principal curvature $C_{2,wl}$ diverges. However, the mean curvature $M_{wl} = (C_{1,wl} + C_{2,wl})/2$ remains finite, since the positive singular contribution from the second principal curvature $C_{2,wl}$ is cancelled by another negative contribution arising from the contour curvature $C_{1,wl}$. This is analogous to the fact that the mean curvature of the catenoid surface is zero. Since the curvature on a smooth vesicle membrane surface varies continuously along an arbitrary direction, the neck curvature of the limiting shape composed of two spherical membrane segments with the radii of R_1 and R_2 (R_1, $R_2 \gg a_{ne}$) is defined as $M_{wl} \approx C_{ne} \equiv \frac{1}{2}\left(\frac{1}{R_1} + \frac{1}{R_2}\right)$.[131,160] Assuming that the membrane has a spontaneous curvature, C_0 ($C_0 \gg C_{ne}$), a constriction force $f_c = 8\pi\kappa\left(\frac{C_0}{2} - C_{ne}\right)$ is generated around the neck.[159] This constriction force is proportional to the curvature difference $\left(\frac{C_0}{2} - C_{ne}\right)$. When this force exceeds the critical force required to break the neck [$\sim$26 pN in the case of ternary GUVs composed of 1-palmitoyl-2-oleoyl-*sn-glycero*-3-phosphocholine (POPC), 1-palmitoyl-2-oleoyl-*sn-glycero*-3-phospho-(1′-*rac*-glycerol) (POPG) and cholesterol (7 : 1 : 2)], the two vesicles of the limiting shape separate, *i.e.*, vesicle division occurs.[159] This critical force is comparable to the constriction force for dynamin of 18–25 pN[236] and FtsZ of 8–80 pN.[237,238] As shown in Fig. 8a, when green fluorescent protein (GFP) was anchored to the outer leaflet of a prolate-shaped phospholipid GUV (POPC : POPG : cholesterol = 7 : 1 : 2, mol ratio) (I), the vesicle deformed into the limiting shape vesicle due to the imposed spontaneous curvature (II). A further increase in the amount of GFP bound to the vesicle resulted in the breaking of the neck and the division of the GUV, as shown in (III).[159] A similar vesicle division induced by the presence of bulky proteins (*e.g.* crescent-shaped BAR domain proteins) on the outer leaflet of vesicle bilayers was observed for several vesicle systems prepared from biological amphiphiles.[239,240]

Another method to attain vesicle division is to introduce a second component amphiphile having an asymmetric molecular shape. The coupling between Gaussian curvature and local lipid composition for binary lipid vesicles destabilize the neck in the limiting shape.[241] The free energy functional, $\Phi[\Omega]$, for the binary vesicle can be expressed as

$$\begin{aligned}\Phi[\Omega] &= \frac{\kappa}{2}\oint \mathrm{d}A(C_1(r) + C_2(r) - C_0)^2 \\ &+ \kappa_G \oint \mathrm{d}A C_1(r)C_2(r) + \lambda \oint \mathrm{d}A C_1(r)C_2(r)\phi(r) \\ &+ \frac{\tau}{2}\oint \mathrm{d}A\phi(r)^2 + \sigma A[\Omega] - pV[\Omega] + \mu \oint \mathrm{d}A\phi(r),\end{aligned} \quad (7)$$

where Ω represents the total surface of the vesicle, $\phi(r)$ is the local area fraction of the minor component lipid. The first and second terms are the same as in eqn (1). The third term expresses the coupling between the Gaussian curvature and the local concentration of membrane molecules through $\lambda = \kappa_G' - \kappa_G$ (κ_G and κ_G' are the Gaussian rigidities of the major and minor component amphiphiles, respectively). The fourth term prefers the homogeneous concentration distribution. σ, p, and μ are the Lagrange multipliers which can be adjusted to achieve the desired vesicle surface (A), vesicle volume (V), and lipid composition. In the case of $\kappa_G' < \kappa_G$, since the neck of the limiting shape vesicle has a negative Gaussian curvature, the minor membrane molecules are excluded from the neck and localized in the spherical part with a positive Gaussian curvature. The segregation of membrane molecules increases the mixing free energy, which stabilizes a state of two separated spherical vesicles rather than a limiting shape vesicle. Therefore, the increase in mixing free energy due to membrane molecule segregation encourages vesicle division.

From an experimental point of view, binary GUVs composed of the cylinder-shaped lipid DPPC and the inverse-cone-shaped lipid DLPE (area fraction of DLPE $\phi_a = 0.2$) showed vesicle reproduction cycles.[222,223] By increasing the temperature of these binary GUVs from 30 °C to 50 °C, the chain melting of DPPC (melting temperature of DPPC, $T_m^{DPPC} = 41$ °C) produced excess surface area. Using this excess area, the binary DPPC/DLPE GUVs showed shape transformations: sphere → prolate → limiting shape, and then the limiting shape vesicle divided into two independent vesicles (Fig. 8b). By decreasing the temperature to 30 °C, the DPPC chains re-ordered, and two spherical daughter vesicles were obtained. When the temperature cycle was repeated, the daughter vesicles produced the next generation of vesicles. Such vesicle reproduction cycles were observed for more than ten generations. This binary DPPC/DLPE vesicle system showed two types of reproduction pathways depending on the composition; for $0.15 < \phi_a < 0.3$, the binary GUVs developed along the budding pathway, whereas for $0.3 < \phi_a < 0.45$, the GUVs transformed along the birthing pathway (Fig. 5-I). Such lipid shape-induced division of binary vesicles composed of cylinder-shaped lipids and inverse-cone-shaped lipids was reproduced *in silico* by coarse-grained molecular dynamics simulation,[242] which is consistent with the theoretical prediction based on eqn (7). It should be noted that the constriction force for this binary vesicle was estimated as $f_c \approx 1$ pN using $\kappa \approx 2 \times 10^{-19}$ J, $C_0 \approx 3 \times 10^5$ m^{-1}, and $C_{ne} \approx 1 \times 10^5$ m^{-1} ($R_1 = R_2 \approx 10$ μm), which is much smaller than the critical force of $\sim$26 pN.[159]

The method of vesicle division driven by the addition of inverse-cone-shaped lipids to vesicles consisting of cylinder-shaped lipids can be applied to other vesicle systems. For example, spherical AOT vesicles grow to prolate shape vesicles (without division) by adding AOT molecules (the same amphiphiles the vesicles are built from), whereas spherical AOT vesicles containing cholesterol or PE lipids grow to a limiting shape after addition of AOT molecules and then show division.[176]

The division of binary vesicles composed of symmetric lipids as well as asymmetric lipids has been observed in many systems. For example, vesicle division was demonstrated in

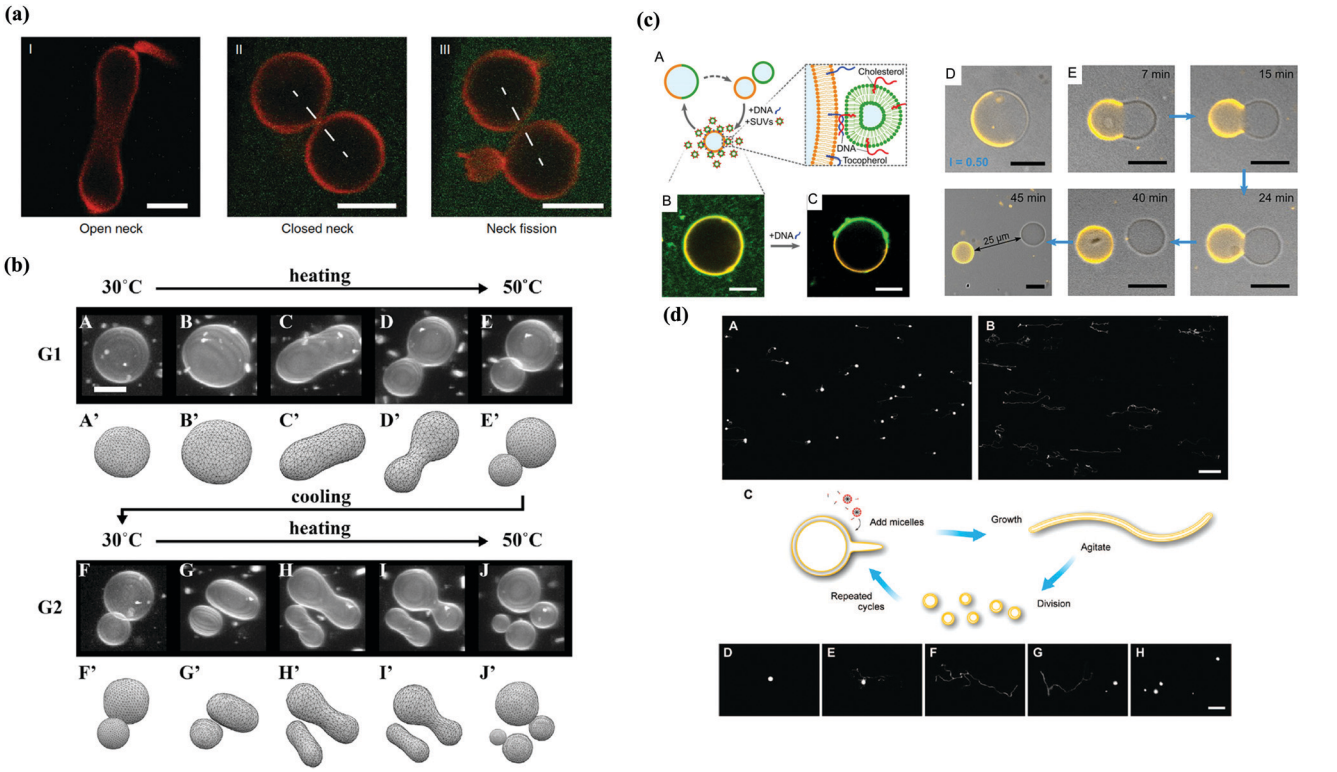

Fig. 8 Examples of experimentally demonstrated divisions of vesicles driven by (a) a change in spontaneous curvature, (b) presence of an inverse cone-shaped lipid, (c) phase separation, and (d) mechanical force. (a) Symmetric division of a single GUV with membrane-bound proteins (GFP with His-tag) into two daughter vesicles. The GUV was prepared from a mixture of POPC, POPG, cholesterol and an anchor lipid that had a His-tag binding unit. The division process starts, in the absence of GFP, from a certain vesicle shape as displayed in I. Addition of GFP then transforms each GUV into two spherical membrane segments that are connected by a closed membrane neck (a limiting shape), as shown in II. A further increase in the GFP concentration leads to the breaking of the neck and to the division of the GUV as shown in III. Scale bars: 5 μm. (This figure is taken from J. Steinkühler *et al.*, *Nat. Commun.*, 2020, **11**, 905; open access article.) (b) Division of a binary spherical GUV consisting of DPPC (cylinder-shaped) and DLPE (inverse cone-shaped), driven by heating-cooling cycles between 30 and 50 °C. (A–E) Deformations of the first-generation vesicle (G1), where the "mother vesicle" produced two "daughter vesicles". (F–J) Second-generation deformations (G2), where the "daughter vesicles" produced "granddaughter vesicles". Scale bar in (A) represents 10 μm. The extracted shapes obtained by relaxing the bending energy at fixed v and $\Delta a = \Delta A/(8\pi d R_0)$ are shown in (A′)–(J′). (Reprinted with permission from T. Jimbo *et al.*, *Biophy. J.*, 2016, **110**, 1551–1562. Copyright 2016 Biophysical Society.) (c) Division and regrowth of phase-separated GUVs consisting of DOPC, cholesterol, DPPC, cardiolipin and DPPE-Rh. (A) Schematic illustration of a programmable vesicle growth and division cycle mediated *via* fusogenic membrane-bound DNA. The zoom image shows the zipper-like arrangement of the DNA, bringing the membranes into close proximity. (B) Representative confocal fluorescence image of a fluorescently labeled Ld-phase (orange) GUV in a feeding bath of Lo SUVs with cholesterol-tagged green-labeled DNA. (C) Addition of complementary tocopherol-tagged DNA leads to SUV fusion and hence the formation of phase-separated vesicles. (D) Overlay of brightfield and confocal images of a phase separated GUV with equally large hemispheres. The Ld phase was labeled with DPPE-Rh (orange color). (E) Confocal fluorescence time series depicting the division process in the presence of invertase. The vesicles are fully separated and quickly diffuse apart after division (see 45 min time point). Scale bars in (B–E): 10 μm. (This figure is taken from Y. Dreher *et al.*, *Angew. Chem., Int. Ed.*, 2021, **133**, 10756; open access article.) (d) Oleic acid/oleate vesicle division triggered by a mild mechanical force. (A and B) Micrographs of vesicle shape transformations during growth, 10 and 30 min after the addition of oleate micelles to multilamellar oleic acid/oleate vesicles. Scale bar, 50 μm. (C) Schematic diagram of cyclic multilamellar vesicle growth and division: vesicles remain multilamellar before and after division. (D–F) Growth of a single multilamellar oleic acid/oleate vesicle, 3 min, 10 min, and 25 min after the addition of oleate micelles, respectively. (G and H) In response to mild fluid agitation, this thread-like vesicle divided into multiple smaller "daughter vesicles". Scale bar for D–H, 20 μm. (Reprinted with permission from T. F. Zhu *et al.*, *J. Am. Chem. Soc.*, 2009, **131**, 5705–5713. Copyright 2009 American Chemical Society.) https://pubs.acs.org/doi/full/10.1021/ja900919c.

binary vesicles composed of PC lipids with two hydrophobic tails and single-chain lyso PC lipids.[183] Similarly, when lyso-PC (16 : 0) was added to binary DPPC/cholesterol vesicles, vesicles with prolate shape deformed into a limiting shape and then showed division.[243,244] For binary POPC/oleic acid vesicles, an increase in pH of the aqueous solution inside the vesicles promoted deprotonation of the oleic acid molecules in the inner leaflet of the bilayer, which resulted in vesicle division.[245] Another example is fatty acid vesicles: when oleic acid/oleate (C18:1) large unilamellar vesicles (LUVs) were added to myristoleic acid/myristoleate (C14:1) multilamellar vesicles (MLVs), many daughter vesicles began to appear, whereas C14:1 MLVs fed with C14:1 LUVs did not show growth or division.[246] Thus, only binary fatty acid vesicles consisting of two types of fatty acids with different hydrocarbon chain lengths exhibited division.

Vesicle division can also be attained on the basis of lipid phase separation within the membrane of multicomponent lipid vesicles. Ternary vesicles composed of saturated phospholipid "A" with a high melting temperature (T_m^A), unsaturated phospholipid "B" with a low melting temperature (T_m^B), and

cholesterol show phase separation into a liquid ordered (L_o) phase rich in phospholipid "A" and a liquid disordered (L_d) phase rich in phospholipid "B".[247] This phase separation forms L_o phase domains in an L_d phase matrix or vice versa, depending on the composition. The geometry of such phase-separated vesicles is theoretically obtained by minimizing the total energy, which is composed of the elastic energy of the membrane and the edge energy of the domains. This theory predicts that flat or weakly curved domains become unstable at a certain limiting domain size and then undergo vesicle budding or division due to the line tension of the domain edge.[248] Line tension-induced vesicle division has been observed frequently in phase-separated phospholipid vesicles.[166,249,250] The shortcoming of the line tension-induced vesicle division is that the composition of the daughter vesicles is different from that of the mother vesicle, which means that recursive vesicle reproduction is difficult to achieve by this mechanism. In this regard, cyclic vesicle reproduction was investigated by combining phase separation-induced vesicle division and fusion for vesicles that consist of "counterpart components", which are absent in the budding domains of the mother vesicles (A in Fig. 8c).[206] In this example, the phase separation of a quaternary vesicle system composed of DPPC, DOPC, cardiolipin, and cholesterol into L_o and L_d phases caused vesicle division, as shown in D and E in Fig. 8c, where the reduced volume of the phase-separated vesicles decreased due to osmotic pressure differences between the vesicle interior and the external solution. The daughter vesicle, which consisted of the L_d phase, was fused with SUVs, which consisted of the L_o phase, by hybridization of template and complementary single strand DNAs anchored to the two types of vesicles (B and C in Fig. 8c). This resulted in a recovery of the initial phase-separated vesicles, *i.e.*, recursive vesicle division was achieved. This study showed that even for vesicle division systems due to lipid phase separation, recursive vesicle division can be attained if the vesicles contain some fusogen. Related to this example are the following experimental observations. A vesicle-trapped aqueous solution can lead to vesicle division based on phase separation: giant vesicles encapsulating an aqueous two-phase system consisting of polyethylene glycol and dextran showed vesicle division by osmotic swelling.[251]

In another approach, vesicle division could be achieved by applying mild mechanical forces.[12,167,173,175,252,253] By adding oleate micelles to multi-lamellar oleic acid vesicles at pH = 8.5, the vesicles grew into thread-like shaped vesicles (Fig. 4D, H and Fig. 8d),[173] whereby the multilamellar vesicles served as reservoir of bilayer-forming lipids. A mild shear stress (>0.35 dynes per cm^2) applied by repeatedly blowing puffs of air induced division of the thread-like vesicles into multiple smaller spherical daughter vesicles. When the daughter vesicles were then fed with micelles, they grew to a "sphere-tail" intermediate stage. Overall, vesicle growth and division cycles could be observed.

2.6. Inflation of vesicles

For a sustainable vesicle reproduction, the daughter vesicles that are produced by vesicle division should not be smaller than the mother vesicle. Therefore, the daughter vesicles must grow into spherical vesicles which have the same size as the mother vesicle. Generally, under conditions of vesicle membrane area enlargement, a simultaneous increase of vesicle volume is due to a flow of water from the external bulk solution into the vesicles, driven by a pressure difference – osmotic or hydrostatic – between vesicle interior and bulk aqueous solution. Since osmosis is relevant for the inflow of water if vesicle reproduction is coupled with a chemical reaction network, in this review we focus on the inflation of vesicles driven by an osmotic pressure difference. In fact, bacterial cells rely on osmosis for water import during cell growth.[254] The volume change ΔV during time Δt is called "inflation" and can be represented by $\frac{\Delta V/v_m}{\Delta t} = -AP_m\Delta c$, where Δc is the concentration difference of an osmolyte across the vesicle membrane, A is the vesicle surface area, P_m is the membrane permeability, and v_m is the molar water volume.[255] However, when the total amount of osmolytes encapsulated inside the vesicle remains constant, the osmotic pressure difference between the inside and outside of the vesicle decreases with time due to the inflow of water, which eventually leads to a cessation of the inflation. Therefore, in order to realize a sustainable volume increase, it is necessary to increase the total amount of osmolyte inside the vesicle in accordance with the volume increase. For example, glycerol penetrates relatively easily from the external solution through fluid phospholipid membranes into the aqueous pool of vesicles formed from such phospholipids. If spherical phospholipid vesicles with encapsulated sucrose solution were placed into a solution that contained both glycerol and oleic acid, the osmotic drag coupled the inflow of glycerol with the inflow of water, causing the vesicle to swell, while oleic acid molecules from the external solution increased the membrane surface area by their incorporation into the membrane to release the membrane tension caused by the swelling.[256,257] If oleic acid molecules are not supplied, the membrane tension caused by vesicle inflation will open a pore in the vesicle membrane.[257–259] Since short-chain fatty acids have relatively high cac values (>10 mM for decanoate),[169] their solutions are suitable reservoirs for inducing inflation of spherical vesicles. Another way to increase the concentration of osmolytes encapsulated inside vesicles is to use chemical or enzymatic decomposition, for example, by entrapping the enzyme invertase inside the vesicles. Invertase catalyses the decomposition of the disaccharide sucrose into the two monosaccharides, fructose and glucose, which increases the osmolarity significantly over time.[206] For a sustainable volume inflation, the osmotic pressure difference between the vesicle interior and the bulk solution must be regulated so that the traffic of osmolytes through the membrane and/or the enzymatic reactions inside the vesicles are strictly controlled.

2.7. Considerations for achieving the reproduction of vesicles as protocell model systems

One of the challenges in preparing a dynamic vesicular compartment system that works according to the key principles of the chemoton model (Fig. 1a) is to achieve vesicle reproduction, either through chemical reactions taking place inside the

vesicles (ideal case) or through membrane-forming molecules that are delivered to preexisting vesicles.

To achieve such vesicle reproduction, it is necessary to realize the process shown in Fig. 2a: (i) incorporation of membrane molecules into the membranes of the mother vesicles that one likes to reproduce; whereby (ii) the incorporated membrane molecules must lead to vesicle growth and a change in vesicle shape to that outward limiting shape vesicles are obtained that finally divide into daughter vesicles; and (iii) the daughter vesicles must recover to the size of the mother vesicles. A sophisticated method for incorporating membrane molecules into vesicles is to synthesise the membrane molecules inside the aqueous pool of the vesicles or within the vesicle membrane. Such vesicle-confined synthesis of membrane-forming molecules has already been achieved successfully by several groups.[180–191] However, these types of advanced methods are difficult to apply for the synthesis of large amounts of membrane molecules. Therefore, in many cases, bilayer membrane-forming molecules are delivered to the vesicles from the external bulk solution. After they are incorporated in the vesicle membrane due to an adjustment of the chemical potential of the molecules to be incorporated, the vesicle membrane grows. One plausible method to adjust the chemical potential of the molecules to be incorporated is to localize a ''counter molecule'' (counter ions or counter polyions) on the vesicle surface which binds to the hydrophilic groups of the membrane molecules in the external solution, and with this reduces their hydrophilicity.[176]

The kinetics of the migration of membrane molecules from one monolayer to the other (lipid ''flip-flop'' or transbilayer lipid diffusion) plays an important role in vesicle reproduction. Assuming that the bilayer-forming molecules are incorporated from the bulk solution into the outer monolayer of spherical mother vesicles, and assuming that the flip-flop rate is much slower than the membrane growth rate, then the grown vesicle would not divide because the area of the inner monolayer would not increase. Only vesicles composed of membrane molecules having an appropriate flip-flop rate can grow to the limiting shape and then divide, but this also requires an increase of the reduced spontaneous curvature expressed by $c_0 = C_0R_0$. Two methods for establishing a spontaneous curvature to the bilayer membrane have been proposed: Either (i) the addition of inverse cone-shaped membrane molecules to vesicles consisting of cylinder-shaped membrane molecules,[222,223] or (ii) the anchoring of bulky polymers (proteins) to the surface of the outer monolayer.[159] In the former case, the coupling of the Gaussian curvature and local density of the inverse cone-shaped membrane molecule destabilizes the membrane neck of the limiting shape vesicle. In the latter case, the large spontaneous curvature causes a strong constriction force that breaks the neck of the limiting shape vesicle. The common feature of both methods is that the deformation of an initially spherical vesicle leads to the formation of an outward limiting shape vesicle, which finally divides into two spherical vesicles (Fig. 2a).

Another important factor for vesicle reproduction is the balance between membrane area growth and volume growth of the vesicles, as demonstrated by Svetina.[260–262] In one specific type of vesicle reproduction process (Fig. 9), the membrane area of a spherical mother vesicle (area A_0, volume V_0, v = 1) increases due to membrane molecules that are incorporated from the external bulk solution, which results in an increase of the internal vesicle volume by permeating water molecules from the external bulk aqueous solution into the vesicle due to a pressure difference between the vesicle interior and the bulk solution. Here the growth rate of the vesicle membrane is expressed by $\frac{dA}{dt} = \frac{\ln 2}{T_d}A$ (T_d: time taken for the membrane to double its area) and the volume growth rate is expressed by $\frac{dV}{dt} = L_p A \Delta P$ (L_p: hydraulic permeability; ΔP: pressures difference between the outside and inside the vesicle). In the phase diagram based on the spontaneous curvature model, the limiting shapes lie on the line L^{pear} (Fig. 2c). Whether the deformation pathway from a sphere can reach the line L^{pear} is determined by the value of the constant $T_d L_p \kappa C_0^4$.[260,263] For $T_d L_p \kappa C_0^4$ = 1.85, the spherical mother vesicle deforms to a symmetric limiting shape composed of two equal spheres ($v = 1/\sqrt{2}$ and $c_0 = 2\sqrt{2}$). Fig. 9 shows the time dependence ($\tau = t/T_d$) of the vesicle volume (V/V_0) and the membrane area (A/A_0) for the vesicle shape transformation from a sphere (point A) to a symmetric limiting shape (point E). Axial cross-sections of some characteristic shapes in Fig. 9 are obtained by minimizing the bending energy. For $T_d L_p \kappa\ C_0^4 >$ 1.85, the mother vesicle deforms to an asymmetric limiting shape composed of two spheres having different radii. This theoretical prediction indicates that the deformation from a

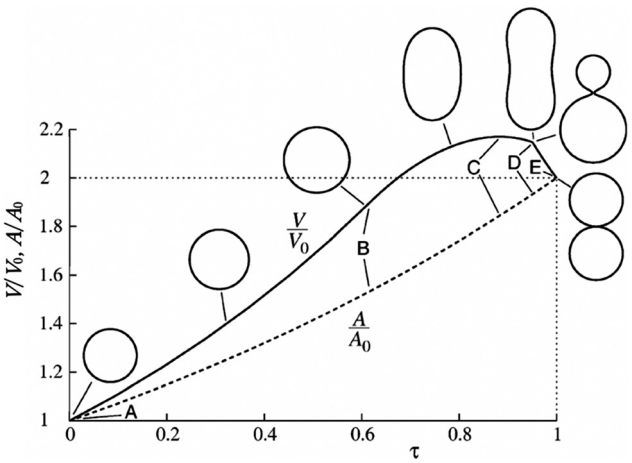

Fig. 9 Vesicle shape transformation from a sphere (point A) to a limiting shape with two identical spheres that are connected through a membrane neck (point E) based on the spontaneous curvature model. Between points A and B, the vesicle grows as a sphere and from point B on, the vesicle shows non-spherical growth. At point C the vesicle reaches the maximum of the bending energy and point D indicates the discontinuous transition from prolate shape to pear shape. Dependence of the relative vesicle volume (full line, V/V_0) and the relative membrane area (dashed line, A/A_0) on the reduced time ($\tau = t/T_d$). Axial cross-sections of some characteristic shapes are also shown. (Reprinted with permission from B. Božič *et al.*, *Eur. Biophys. J.*, 2004, **33**, 565–571. Copyright 2004 EBSA. The *y* axis label (V/V_0 and A/A_0) was added.)

spherical shape to a limiting shape requires that the membrane growth rate, the membrane water permeability, the spontaneous membrane curvature, and the bending rigidity are controlled to satisfy the inequality $T_d L_p \kappa C_0^4 \geq 1.85$ during the deformation.[262] Especially, sustained vesicle reproduction requires sustained vesicle growth. Since the volume growth rate is determined by the osmotic pressure difference between the inside and outside of the vesicle, the osmotic pressure difference demands to be kept constant. In most cases, however, keeping a constant osmotic pressure difference is difficult due to dilution of the osmolytes. Therefore, it is necessary to keep the concentration of the osmolytes inside the vesicle to expand the vesicle volume by synthesis of the osmolytes inside the vesicle or by uptake of the osmolytes from the external solution. This is an issue that needs to be addressed in future work.

3. Coupling of vesicle reproduction with information transfer

Research on vesicle reproduction has progressed thanks to efforts by different research groups. However, in order to develop a vesicle reproduction system into an autonomous system that is conceptually as similar as possible to a living system, it is necessary to couple vesicle reproduction with information transfer,[23] whereby the information molecule should encode information for vesicle reproduction and for the replication of itself.[35,264] Here we introduce two approaches for coupling vesicle reproduction and information transfer: a top-down type approach that mimics the central dogma of contemporary biological systems and a bottom-up type in which an information polymer promotes vesicle growth. Although it is a mystery how information transfer and cellular compartment reproduction were coupled in early cells or protocells on the primitive Earth, the two approaches discussed in the following can be considered as starting points for exploring the pathway from vesicles to protocells and minimal cells.

In all contemporary biological cells, the information for the synthesis of the proteins (enzymes) that are responsible for the synthesis of membrane molecules is encoded in the base sequence of DNA molecules (as for any other proteins of the cells). DNA is a highly sophisticated macromolecular information molecule. DNA base sequences are converted into amino acid sequences of proteins *via* RNA. Together with other enzymes – and the necessary low molar mass building blocks – cell reproduction and replication of the information molecules are achieved. In order to understand the key steps of the cell reproduction process, a plausible approach is to reconstruct a pathway from glucose to lipids using proteins expressed by DNA inside a vesicle and to try to realize vesicle reproduction (Fig. 1b). This approach was first attempted by synthesising PC lipids in soybean PC vesicles using four enzymes of the salvage pathway for PC synthesis, G3P-AT (*sn-glycerol*-3-phosphate acyltransferase), LPA-AT (l-acyl-*sn-glycerol*-3-phosphate acyltransferase), PA-P (phosphatidate phosphatase), and CDPC-PT (cytidinediphosphocholine phosphocholinetransferase).[265] Then, Kuruma *et al.* succeeded in synthesising two membrane proteins involved in the salvage pathway, G3P-AT and LPA-AT, using a totally reconstructed cell-free protein expression system (PURE, Protein synthesis Using Recombinant Elements[266]) encapsulated in lipid vesicles.[267] In another work, the reconstruction of a pathway that converts glucose to fatty acids (decanoic acid, lauric acid, myristic acid, and palmitic acid) *in vitro* was successful by using 30 purified proteins expressed from *E. coli* DNA, although the formation of membranes from the synthesised fatty acids was difficult.[268,269] On the other hand, several approaches were undertaken to grow vesicles by synthesising various phospholipids from glycerol-3-phosphate (G3P) and acetyl-CoA within a vesicle.[270–272] The model plasmid, pGEMM7Δpsd, was expressed using the PURE system[266] within giant vesicles composed of DOPC/DOPE/DOPG/cardiolipin to produce glycerol 3-phosphate acyltransferase (PlsB = G3P-AT), lysophosphatidic acid acyltransferase (PlsC = LPA-AT), cytidine diphosphate-diacylglycerol synthase (CDsA), and phosphatidylserine synthase (PssA), the latter catalysing the formation of phosophatidylserine (PS) from acyl-CoA and G3P (Fig. 10-Ia). The PS synthesised in the vesicle membrane binds to the green fluorescent dye LactC2-eGFP in the external solution, resulting in the accumulation of a GFP signal in PS-enriched vesicles. Analysis of confocal laser scanning microscopy images of a giant vesicle (initially labelled with a dye that yields magenta fluorescence) showed that a clear increase in the LactC2-eGFP signal with the growth of the vesicle between 0.5 and 6 h occurred, indicating that the synthesis of 1,2-dioleoyl-*sn-glycero*-3-phosphocholine (DOPS) from oleoyl-CoA took place[272] (Fig. 10-Ib).

In other recent approaches, non-natural vesicle reproduction systems were developed. This type of work does not aim to copy a biological system by using the same chemical compounds and reactions of biological systems but aims to assemble a synthetic vesicle compartment system that conceptually captures the key features of the biological cells in their artificial design. The main challenge in this approach is to prepare a vesicle reproduction system of any type, where vesicle reproduction is directly coupled to an information molecule. The pioneering work was performed by Sugawara's group.[273] The vesicle membrane-forming amphiphile synthesised and used was the same as the one shown in Fig. 5-II, the cationic membrane molecule V, but this time the giant vesicles contained an encapsulated DNA amplification system. The vesicle-trapped DNA was amplified by the PCR technique, whereby the vesicles also showed growth and division behaviour after the addition of a vesicular membrane precursor molecule (Fig. 10-II). The amplified DNA was distributed among the daughter giant vesicles. In particular, the amplification of the DNA accelerated the division of the giant vesicles, which means that self-replication of the vesicle-trapped informational compound (DNA) was linked to the self-reproduction of the compartment through an interplay between DNA and the cationic vesicular membrane. This link between vesicle reproduction and DNA replication was demonstrated by showing a dependence of the vesicle division mode on the length of the DNA.[274] This system was further developed to a recursive self-proliferation system, where the vesicles were fed with the ingredients that were consumed during the reproduction and replication processes through a pH-induced fusion of conveyer vesicles containing these depleted ingredients.[275]

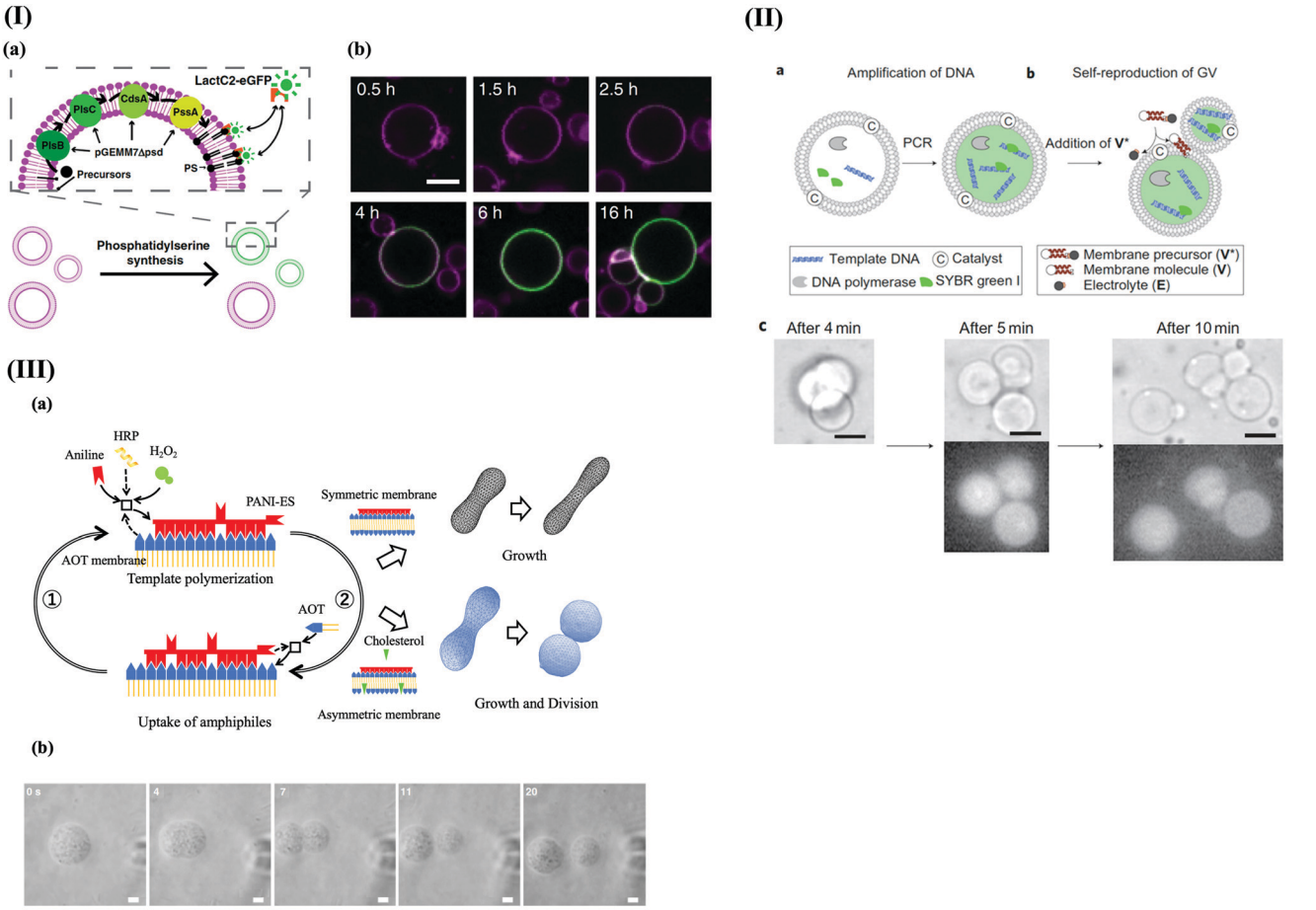

Fig. 10 Vesicle reproduction coupled with information transfer. (I) Membrane growth driven by genetically controlled phospholipid synthesis. (a) Schematic representation of gene expression-coupled phosphatidylserine (PS) biosynthesis, where PS-producing enzymes (PlsB, PlsC, CdsA and PssA) encoded in a synthetic minigenome (pGEMM7Δpsd) are cell-free expressed within giant unilamellar lipid vesicle compartments. The GUVs were prepared from DOPC, DOPE, DOPG, cardiolipid, DPPE-Texas Red, and DSPE-PEG-biotin. The enzymes catalyse the formation of PS from acyl-CoA and G3P. Membrane-exposed PS recruits the fluorescent reporter LactC2-eGFP, resulting in accumulated GFP signal in PS-enriched liposomes. (b) Time-lapse images of a liposome exhibiting increasing LactC2-eGFP signal over time. Scale bar: 5 μm. (This figure is taken from D. Blanken *et al.*, (2020) *Nat. Commun.*, 2020, **11**, 4317; open access article.) (II) Schematic representation of an example for a chemical link between amplification of DNA and self-reproduction of giant vesicles (GVs); for the chemical structures of the amphiphile V used and its precursor V*, see (Fig. 5-II). (a) Amplification of DNA within a GV containing PCR reagents (template DNA, primers, fluorescent tag SYBR Green I, deoxynucleoside triphosphates, DNA polymerase and Mg^{2+}). (b) Vesicular self-reproduction induced by adding membrane precursor V*. Addition of V* produces membrane molecules (V) and electrolytes (E) through hydrolysis assisted by an amphiphilic catalyst. Adhesion of the amplified DNA to the inner leaflet accelerates vesicular growth and division. (c) Real-time light microscopy observation of morphological changes of DNA-amplified GVs after addition of V*. Original GVs began to grow and divide 4 min after adding V*. Complete division into four GVs occurred at 5.5 min, and separation occurred at 7 min (top panels). Partition of DNA was detected using fluorescence microscopy (bottom panels). Scale bars: 10 μm. (Reprinted with permission from K. Kurihara *et al.*, *Nat. Chem.*, 2011, **3**, 775–781. Copyright 2011 Springer Nature.) (III) General scheme of vesicle reproduction linked with a synthetic information polymer. (a) This system consists of the "vesicle template"-assisted enzymatic polymerisation of aniline occurring on the surface of AOT vesicles and the selective uptake of AOT molecules from the external solution by the vesicles through interactions with PANI-ES. In the drawing, solid arrows indicate the participation of reactants and the products of the reaction; dashed arrows indicate the promotion of the reaction; boxes represent reactions, and double line arrows (1 and 2) indicate the mutual promotion in the system. The mutual promotion results in vesicle growth for vesicles composed of AOT only and vesicle growth and division for binary vesicles composed of AOT and cholesterol. (b) Phase contrast light microscopy images of a binary AOT/cholesterol GUV, taken during the polymerisation reaction. The binary AOT/cholesterol GUV coupled with the synthesis of PANI-ES, showed vesicle growth by uptake of AOT molecules present in the external solution and then vesicle division. Length of the scale bars: 5 μm. (This figure is taken from M. Kurisu *et al.*, *Commun. Chem.*, 2019, **2**, 117; open access article.)

In the study just mentioned, DNA was used as information molecule. This DNA, however, did not encode the information for making the membrane molecules. In another, completely different set of experiments, vesicle reproduction system using a synthetic polymer was recently developed, as shown in Fig. 10-III (see also the Section "2.5. Division of vesicles").[176] The polymer used was PANI-ES, the cationic emeraldine salt form of polyaniline. PANI-ES associates with bilayer membranes formed by negatively charged AOT molecules. With this physico-chemical property of PANI-ES, PANI-ES encodes information about the binding to AOT molecules. PANI-ES is obtained on the surface of AOT vesicles from aniline with the help of the enzyme horseradish peroxidase (HRP) and hydrogen peroxide as oxidant. The vesicles act as a kind of template and promote the polymerisation

in such a way that mainly linear *para*-NC coupling of the monomer aniline occurs (with minimal chain branching); with this, a defined ''sequence'' in polyaniline is obtained (corresponding to the half oxidized and half reduced tetraaniline repeating unit of PANI-ES).[276,277] This PANI-ES formation and binding to the AOT vesicle membrane is coupled to (PANI-ES) N–H···O= S (AOT) hydrogen bonding, steric or electrostatic interactions.[278,279] If AOT micelles are added during the HRP-catalysed polymerisation reaction, the AOT-PANI-ES vesicles interact with the AOT molecules present in the external solution and selectively incorporate them into the vesicle membrane, which leads to vesicle growth. The characteristic feature of this system is that polyaniline can also be synthesised in the presence of vesicles composed of membrane molecules other than AOT, such as anionic or neutral phospholipids. In this case, however, the structure of the polymer molecules obtained, *i.e.*, the coupling way of the monomer units and the oxidation state of the polymeric product, is different from PANI-ES, *i.e.*, less uniform and more random (mixture of *ortho*- and *para*-couplings, with the formation of branched units). The vesicles do not grow in these cases, even if phospholipids or AOT molecules are added from the external solution. Thus, AOT-based vesicles encourage the synthesis of PANI-ES and PANI-ES promotes the growth of AOT vesicles based on the ''sequence'' information of PANI-ES. As mentioned in the Section ''2.5. Division of vesicles'', if the AOT vesicles also contain cholesterol or phosphatidylethanolamine (PE) lipids, the vesicles show not only growth but also reproduction (Fig. 10-IIIa and b). Although this system uses molecules that are quite different from those of biological cells, this model compartment system consists of cycles that resemble two cycles of the chemoton model, the genetic and the membrane cycles, see Fig. 1a.

In this last example, vesicle reproduction is controlled by information polymer molecules that are synthesised by a mechanism – ''template polymerisation'' – that is conceptually related to DNA/RNA template polymerisation in contemporary living system. Another approach is the basis of the micelle-based protocell model, which was proposed by Lancet (called GARD, ''graded autocatalysis replication domain'').[121] This model relies on the molecular composition of dynamic micellar aggregates. The stability of the micellar aggregates is determined by the adsorption and desorption rates of the amphiphiles, which are influenced by the type and amounts of other amphiphiles present in the aggregate. Thus, the micelle composition carries a kind of genetic information that determines the proliferation ability.[120–122] The GARD model describes the kinetics of molecular assemblies (micelles) composed of amphiphilic molecules that might have been present in the primordial soup.

4. Outlook

In this review, living systems are considered as systems composed of reproducing functionalized vesicles as membrane-bounded compartments maintained by metabolic reaction networks regulated by a flow of sequence information implemented in macromolecules. While this is a highly simplified view of what living forms of matter are, it may help to further develop our current understanding of biological cells in their living state as dynamic non-equilibrium compartment systems. The preparation of artificial vesicular reproduction systems is a major goal of protocell and minimal cell research. Thanks to the recent developments in synthetic biology, synthetic and systems chemistry, as well as soft matter physics, the origin-of-life research community working on potentially prebiotic compartment systems is moving towards this goal. Nevertheless, the ultimate goal, *i.e.*, constructing an autonomous and sustainable vesicular compartment system, is still far away from its realisation. Future fundamental research in the area of systems chemistry and membrane biophysics will show how close to the goal one will be able to move.

As mentioned in this review, for achieving vesicle reproduction *in vitro*, two main approaches are being undertaken. One is the reconstruction of a membrane lipid synthesis pathway using the same DNA–RNA–protein systems contemporary forms of life use,[267,270–272,280] another one aims at realizing the reproduction of vesicles on the basis of information molecules and/or with vesicle systems that are built from components that are completely different from the ones of biological systems.[176,273]

In the first case, a pathway that converts glucose to fatty acids using 30 purified proteins[269] and a pathway that synthesizes phospholipids from G3P and acetyl-CoA using 7 plasmid encoded genes for the synthesis of phospholipids[265] were reconstructed successfully. However, it has been shown that even to maintain a ''simple'' bacterial system, as many as $\sim$250 essential genes must be expressed, with the additional requirement that the expressed proteins must cooperate in a spatially and timely correct way.[20,21] A plausible next goal in this area of research may be to copy vesicle reproduction by reconstructing the phospholipid synthesis pathway associated with glycolysis.

In the second case, AOT vesicle reproduction was achieved in conjunction with ''template'' polymerization, which encodes the information for membrane molecules to be incorporate into the vesicle membrane.[176] However, this type of ''template'' polymerization produces only one type of polymer (PANI-ES) that promotes membrane growth; moreover, other molecules that are essential to maintain vesicle reproduction are supplied from the external solution (importance of the presence of an inverted cone-shaped molecule). For an autonomous and sustainable vesicle reproduction system, however, such essential molecules should be synthesised by a reaction network inside the vesicles. In addition, new segments should be introduced in the polymer structure so that the information polymer could encode additional information for the vesicle reproduction process. Thus, the realisation of a ''minimal cell system'' containing metabolic, genetic, and membrane cycles should be the next target in this research.

The path from simple molecules and molecular assemblies to protocells and minimal cells is long and involves many demanding experimental challenges. This does not seem very surprising, since the emergence of the first cells on the early Earth from organic molecules and inorganic compounds seems to have taken hundreds of millions of years, under conditions

very different from those prevailing on Earth today. Even if the lofty goals of many research teams cannot be achieved, the hope is that the investigations and advances in this field will contribute to a better understanding of living systems and their possible emergence from the non-living. New and unconventional ideas are in demand.

Conflicts of interest

There are no conflicts to declare.

Acknowledgements

We would like to acknowledge financial support from JSPS KAKENHI, Grant Number: JP20H00120.

References

1 B. Alberts, A. Johnson, J. Lewis, D. Morgan, M. Raff, K. Roberts and P. Walter, *Molecular Biology of the Cell*, Garland Science, New York, 6th edn, 2014.
2 K. Ruiz-Mirazo, C. Briones and A. de la Escosura, *Chem. Rev.*, 2014, **114**, 285–366.
3 G. Ashkenasy, T. M. Hermans, S. Otto and A. F. Taylor, *Chem. Soc. Rev.*, 2017, **46**, 2543–2554.
4 A. Lopez and M. Fiore, *Life*, 2019, **9**, 49.
5 M. Doi, *Soft Matter Physics*, Oxford University Press, Oxford, 2013.
6 S. A. Safran, *Statistical Thermodynamics of Surfaces, Interfaces, and Membranes*, CRC Press, Boca Raton, 2018.
7 P. G. De Gennes, F. Brochard-Wyart and D. Quéré, *Capillarity and Wetting Pphenomena: Drops, Bubbles, Pearls, Waves*, Springer, New York, 2004.
8 J. D. Sutherland, *Angew. Chem., Int. Ed.*, 2016, **55**, 104–121.
9 C. Bonfio, D. A. Russell, N. J. Green, A. Mariani and J. D. Sutherland, *Chem. Sci.*, 2020, **11**, 10688–10697.
10 H. J. Morowitz, B. Heinz and D. W. Deamer, *Orig. Life Evol. Biosph.*, 1988, **18**, 281–287.
11 P. A. Monnard and D. Deamer, *Anatom. Rec.*, 2002, **268**, 196–207.
12 K. Adamala and J. W. Szostak, *Nat. Chem.*, 2013, **5**, 495.
13 P. A. Monnard and P. Walde, *Life*, 2015, **5**, 1239–1263.
14 P. Dalai and N. Sahai, in *Handbook of Astrobiology*, ed. V. M. Kolb, CRC Press, Boca Raton, 2019, pp. 491–517.
15 I. Gözen, E. S. Köksal, I. Põldsalu, L. Xue, K. Spustova, E. Pedrueza-Villalmanzo, R. Ryskulov, F. Meng and A. Jesorka, *Small*, 2022, **18**, 2106624.
16 T. Gánti, *J. Theor. Biol.*, 1997, **187**, 583–593.
17 T. Gánti, *The principles of life*, Oxford University Press, Oxford, 2003.
18 J. Griesemer, *J. Theor. Biol.*, 2015, **381**, 23–28.
19 L. Bich and S. Green, *Synthese*, 2018, **195**, 3919–3946.
20 E. V. Koonin, *Annu. Rev. Genom. Hum. Genet.*, 2000, **1**, 99–116.
21 P. Xu, X. Ge, L. Chen, X. Wang, Y. Dou, J. Z. Xu, J. R. Patel, V. Stone, M. Trinh, K. Evans, T. Kitten, D. Bonchev and G. A. Buck, *Sci. Rep.*, 2011, **1**, 125.
22 F. Crick, *Nature*, 1970, **227**, 561–563.
23 J. W. Szostak, D. P. Bartel and P. L. Luisi, *Nature*, 2001, **409**, 387–390.
24 P. L. Luisi, *The Emergence of Life–From Chemical Origins to Synthetic Biology*, Cambridge University Press, Cambridge, 2006.
25 *Protocells–Bridging Nonliving and Living Matter*, ed. S. Rasmussen, M. A. Bedau, L. Chen, D. Deamer, D. C. Krakauer, N. H. Packard and P. F. Stadler, MIT Press, Cambridge, 2008.
26 *The Origins of Life*, ed. D. Deamer and J. W. Szostak, Cold Spring Harbor Laboratory Press, New York, 2010.
27 D. Deamer, *First Life-Discovering the Connections Between Stars, Cells, and How Life Began*, University of California Press, Berkeley, 2011.
28 *The Minimal Cell: The Biophysics of Cell Compartment and the Origin of Cell Functionality*, ed. P. L. Luisi and P. Stano, Springer, Heidelberg, 2011.
29 S. S. Mansy, *Int. J. Mol. Sci.*, 2009, **10**, 835–843.
30 J. P. Schrum, T. F. Zhu and J. W. Szostak, *Cold Spring Harb. Perspect. Biol.*, 2010, **2**, a002212.
31 I. A. Chen and P. Walde, *Cold Spring Harb. Perspect. Biol.*, 2010, **2**, a002170.
32 P. Stano and P. L. Luisi, *Chem. Comm.*, 2010, **46**, 3639–3653.
33 P. Stano, P. Carrara, Y. Kuruma, T. P. de Souza and P. L. Luisi, *J. Mater. Chem.*, 2011, **21**, 18887–18902.
34 S. A. Kauffman, *Life*, 2011, **1**, 34–48.
35 V. Noireaux, Y. T. Maeda and A. Libchaber, *Proc. Natl. Acad. Sci. U. S. A.*, 2011, **108**, 3473–3480.
36 F. Caschera and V. Noireaux, *Curr. Opin. Chem. Biol.*, 2014, **22**, 85–91.
37 P. Walde, H. Umakoshi, P. Stano and F. Mavelli, *Chem. Comm.*, 2014, **50**, 10177–10197.
38 J. C. Blain and J. W. Szostak, *Annu. Rev. Biochem.*, 2014, **83**, 615–640.
39 A. Pressman, C. Blanco and I. A. Chen, *Curr. Biol.*, 2015, **25**, R953–R963.
40 S. Rasmussen, A. Constantinescu and C. Svaneborg, *Philos. Trans. R. Soc. Lond., B, Biol. Sci.*, 2016, **371**, 20150440.
41 D. Deamer, *Life*, 2017, **7**, 5.
42 J. W. Szostak, *Angew. Chem., Int. Ed.*, 2017, **56**, 11037–11043.
43 P. Schwille, J. Spatz, K. Landfester, E. Bodenschatz, S. Herminghaus, V. Sourjik, E. Tobias, P. Bastiaens, R. Lipowsky, A. Hyman, P. Dabrock, J.-C. Baret, T. Vidakovic-Koch, P. Bieling, R. Dimova, H. Mutschler, T. Robinson, D. Tang, S. Wegner and K. Sundmacher, *Angew. Chem., Int. Ed.*, 2018, **57**, 13382–13392.
44 D. Lancet, R. Zidovetzki and O. Markovitch, *J. R. Soc., Interface*, 2018, **15**, 20180159.
45 O. D. Toparlak and S. S. Mansy, *Exp. Biol. Med.*, 2019, **244**, 304–313.
46 M. Imai and P. Walde, in *The Giant Vesicle Book*, ed. R. Dimova and C. Marques, CRC Press, Boca Raton, 2020, pp. 569–583.
47 B. Ghosh, R. Bose and T. D. Tang, *Curr. Opin. Colloid Interface Sci.*, 2020, **52**, 101415.

48 N. J. Gaut and K. P. Adamala, *Adv. Biol.*, 2021, **5**, 2000188.
49 K. A. Podolsky and N. K. Devaraj, *Nat. Rev. Chem.*, 2021, **5**, 676–694.
50 F. H. Crick, *J. Mol. Biol.*, 1968, **38**, 367–379.
51 W. Gilbert, *Nature*, 1986, **319**, 618.
52 E. O. Leslie, *Crit. Rev. Biochem. Mol. Biol.*, 2004, **39**, 99–123.
53 P. G. Higgs and N. Lehman, *Nat. Rev. Genet.*, 2015, **16**, 7–17.
54 B. H. Patel, C. Percivalle, D. J. Ritson, C. D. Duffy and J. D. Sutherland, *Nat. Chem.*, 2015, **7**, 301–307.
55 G. F. Joyce and J. W. Szostak, *Cold Spring Harb. Perspect. Biol.*, 2018, **10**, a034801.
56 S. Becker, J. Feldmann, S. Wiedemann, H. Okamura, C. Schneider, K. Iwan, A. Crisp, M. Rossa, T. Amatov and T. Carell, *Science*, 2019, **366**, 76–82.
57 K. F. Tjhung, M. N. Shokhirev, D. P. Horning and G. F. Joyce, *Proc. Natl. Acad. Sci. U. S. A.*, 2020, **117**, 2906–2913.
58 S. C. Kim, L. Zhou, W. Zhang, D. K. O'Flaherty, V. Rondo-Brovetto and J. W. Szostak, *J. Am. Chem. Soc.*, 2020, **142**, 2317–2326.
59 S. C. Kim, D. K. O'Flaherty, C. Giurgiu, L. Zhou and J. W. Szostak, *J. Am. Chem. Soc.*, 2021, **143**, 3267–3279.
60 G. Zubay, *Origins of Life on the Earth and in the Cosmos*, Academic Press, San Diego, 2000.
61 D. Braun and A. Libchaber, *Phys. Rev. Lett.*, 2002, **89**, 188103.
62 J. P. Ferris, *Orig. Life Evol. Biosph*, 2002, **32**, 311–332.
63 B. Damer and D. Deamer, *Astrobiology*, 2020, **20**, 429–452.
64 W. Martin, J. Baross, D. Kelley and M. J. Russell, *Nat. Rev. Microbiol.*, 2008, **6**, 805–814.
65 P. Baaske, F. M. Weinert, S. Duhr, K. H. Lemke, M. J. Russell and D. Braun, *Proc. Natl. Acad. Sci. U. S. A.*, 2007, **104**, 9346–9351.
66 M. Kreysing, L. Keil, S. Lanzmich and D. Braun, *Nat. Chem.*, 2015, **7**, 203–208.
67 M. Eigen and P. Schuster, *Naturwissenschaften*, 1977, **64**, 541–565.
68 M. Eigen and P. Schuster, *Naturwissenschaften*, 1978, **65**, 7–41.
69 M. Eigen and P. Schuster, *Naturwissenschaften*, 1978, **65**, 341–369.
70 S. Toyabe and D. Braun, *Phys. Rev. X*, 2019, **9**, 011056.
71 S. Wright, *Proceedings of the Sixth International Congress on Genetics*, 1932, vol. 1, pp. 356–366.
72 J. A. G. De Visser and J. Krug, *Nat. Rev. Genet.*, 2014, **15**, 480–490.
73 S. Kauffman and S. Levin, *J. Theor. Biol.*, 1987, **128**, 11–45.
74 S. A. Kauffman and E. D. Weinberger, *J. Theor. Biol.*, 1989, **141**, 211–245.
75 S. S. Athavale, B. Spicer and I. A. Chen, *Curr. Opin. Chem. Biol.*, 2014, **22**, 35–39.
76 A. D. Pressman, Z. Liu, E. Janzen, C. Blanco, U. F. Müller, G. F. Joyce, R. Pascal and I. A. Chen, *J. Am. Chem. Soc.*, 2019, **141**, 6213–6223.
77 W. V. Allen and C. Ponnamperuma, *BioSystems*, 1967, **1**, 24–28.
78 T. M. McCollom, G. Ritter and B. R. Simoneit, *Orig. Life Evol. Biosph*, 1999, **29**, 153–166.
79 A. I. Rushdi and B. R. Simoneit, *Orig. Life Evol. Biosph*, 2001, **31**, 103–118.
80 H. Mißbach, B. C. Schmidt, J. P. Duda, N. K. Lünsdorf, W. Goetz and V. Thiel, *Org. Geochem.*, 2018, **119**, 110–121.
81 M. P. Joshi, A. A. Sawant and S. Rajamani, *Chem. Sci.*, 2021, **12**, 2970–2978.
82 P. Van Der Gulik, S. Massar, D. Gilis, H. Buhrman and M. Rooman, *J. Theor. Biol.*, 2009, **261**, 531–539.
83 E. T. Parker, H. J. Cleaves, J. P. Dworkin, D. P. Glavin, M. Callahan, A. Aubrey, A. Lazcano and J. L. Bada, *Proc. Natl. Acad. Sci. U. S. A.*, 2011, **108**, 5526–5531.
84 M. Rodriguez-Garcia, A. J. Surman, G. J. Cooper, I. Suárez-Marina, Z. Hosni, M. P. Lee and L. Cronin, *Nat. Commun.*, 2015, **6**, 8385.
85 R. Pascal and I. A. Chen, *Nat. Chem.*, 2019, **11**, 763–764.
86 P. J. Bracher, *Nat. Chem.*, 2015, **7**, 273–274.
87 R. Koningsveld, W. H. Stockmayer and E. Nies, *Polymer Phase Diagrams: A Textbook*, Oxford University, New York, 2001.
88 R. R. Poudyal, R. M. Guth-Metzler, A. J. Veenis, E. A. Frankel, C. D. Keatin and P. C. Bevilacqua, *Nat. Commun.*, 2019, **10**, 490.
89 B. Drobot, J. M. Iglesias-Artola, K. Le Vay, V. Mayr, M. Kar, M. Kreysing, H. Mutschler and T.-Y. D. Tang, *Nat. Commun.*, 2018, **9**, 3643.
90 T. Beneyton, C. Love, M. Girault, T.-Y. D. Tang and J.-C. Baret, *ChemSystemsChem*, 2020, **2**, e2000022.
91 I. B. A. Smokers, M. H. I. van Haren, T. Lu and E. Spruijt, *ChemSystemsChem*, 2022, **4**, e202200004.
92 D. Garenne, L. Beven, L. Navailles, F. Nallet, E. J. Dufourc and J.-P. Douliez, *Angew. Chem., Int. Ed.*, 2016, **55**, 13475–13479.
93 N. Martin and J.-P. Douliez, *ChemSystemsChem*, 2021, **3**, e2100024.
94 J. R. Vieregg and T.-Y. D. Tang, *Curr. Opin. Colloid Interface Sci.*, 2016, **26**, 50–57.
95 A. Ianeselli, D. Tetiker, J. Stein, A. Kühnlein, C. B. Mast, D. Braun and T.-Y. D. Tang, *Nat. Chem.*, 2022, **14**, 32–39.
96 P. A. Bachmann, P. L. Luisi and J. Lang, *Nature*, 1992, **357**, 57–59.
97 D. Lancet, R. Zidovetzki and O. Markovitch, *J. R. Soc., Interface*, 2018, **15**, 20180159.
98 A. I. Oparin and K. L. Gladilin, *BioSystems*, 1980, **12**, 133–145.
99 A. I. Oparin, *Origin of Life*, Dover, New York, 2003.
100 S. Koga, D. S. Williams, A. W. Perriman and S. Mann, *Nat. Chem.*, 2011, **3**, 720–724.
101 P. Walde, *Orig. Life Evol. Biosph.*, 2006, **36**, 109–150.
102 M. M. Hanczyc and P. A. Monnard, *Lipid Technol.*, 2016, **28**, 88–92.
103 R. A. Black, M. C. Blosser, B. L. Stottrup, R. Tavakley, D. W. Deamer and S. L. Keller, *Proc. Natl. Acad. Sci. U. S. A.*, 2013, **110**, 13272–13276.
104 R. A. Black and M. C. Blosser, *Life*, 2016, **6**, 33.
105 C. E. Cornell, R. A. Black, M. Xue, H. E. Litz, A. Ramsay, M. Gordon, A. Mileant, Z. R. Cohen, J. A. Williams, K. K. Lee, G. P. Drobny and S. L. Keller, *Proc. Natl. Acad. Sci. U. S. A.*, 2019, **116**, 17239–17244.

106 K. Kruger, P. J. Grabowski, A. J. Zaug, J. Sands, D. E. Gottschling and T. R. Cech, *Cell*, 1982, **31**, 147–157.
107 W. K. Johnston, P. J. Unrau, M. S. Lawrence, M. E. Glasner and D. P. Bartel, *Science*, 2001, **292**, 1319–1325.
108 T. A. Lincoln and G. F. Joyce, *Science*, 2009, **323**, 1229–1232.
109 N. Lee, Y. Bessho, K. Wei, J. W. Szostak and H. Suga, *Nat. Struct. Biol.*, 2000, **7**, 28–33.
110 L. Sun, Z. Cui, R. L. Gottlieb and B. Zhang, *Chem. Biol.*, 2002, **9**, 619–628.
111 E. J. Hayden, G. von Kiedrowski and N. Lehman, *Angew. Chem., Int. Ed.*, 2008, **120**, 8552–8556.
112 H. F. Noller, *Cold Spring Harb. Perspect. Biol.*, 2012, **4**, a003681.
113 A. J. Bissette and S. P. Fletcher, *Angew. Chem., Int. Ed.*, 2013, **52**, 12800–12826.
114 S. Kauffman, *J. Theor. Biol.*, 1986, **119**, 1–24.
115 S. Kauffman, *Origins of Order: Self Organization and Selection in Evolution*, Oxford University Press, New York, 1993.
116 W. Hordijk and M. Steel, *J. Theor. Biol.*, 2004, **227**, 451–461.
117 J. C. Xavier, W. Hordijk, S. Kauffman, M. Steel and W. F. Martin, *Proc. R. Soc. B*, 2020, **287**, 20192377.
118 S. S. Luginbühl, K. R. Mirazo, R. Ostaszewski, F. Gallou and P. Walde, *Nat. Rev. Chem.*, 2018, **2**, 306–327.
119 A. Küchler, M. Yoshimoto, S. Luginbühl, F. Mavelli and P. Walde, *Nat. Nanotechnol.*, 2016, **11**, 409–420.
120 D. Segré, D. Ben-Eli, D. W. Deamer and D. Lancet, *Orig. Life Evol. Biosph*, 2001, **31**, 119–145.
121 D. Segré and D. Lancet, *Chemtracts*, 1999, **12**, 382–397.
122 A. Kahana and D. Lancet, *Nat. Rev. Chem.*, 2021, **5**, 870–878.
123 R. Rubio-Sánchez, D. K. O'Flaherty, A. Wang, F. Coscia, G. Petris, L. Di Michele, P. Cicuta and C. Bonfio, *J. Am. Chem. Soc.*, 2021, **143**, 16589–16598.
124 W. Helfrich, *Z. Naturforsch. C*, 1973, **28**, 693–703.
125 U. Seifert, K. Berndl and R. Lipowsky, *Phys. Rev. A*, 1991, **44**, 1182–1202.
126 B. Božič, S. Svetina, B. Žekš and R. E. Waugh, *Biophys. J.*, 1992, **61**, 963–973.
127 W. Wiese, W. Harbich and W. Helfrich, *J. Condens. Matter Phys.*, 1992, **4**, 1647–1657.
128 U. Seifert, L. Miao, H. G. Döbereiner and M. Wortis, *Springer Proc. Phys.*, 1992, **66**, 93–96.
129 U. Seifert, *Adv. Phys.*, 1997, **46**, 13–137.
130 S. A. Pandit and H. L. Scott, in *Soft Matter, Volume 4: Lipid Bilayers and Red Blood Cells*, ed. G. Gompper and M. Schick, Wiley-VCH, Weinheim, 2008, pp. 1–82.
131 R. Lipowsky, in *The Giant Vesicle Book*, ed. R. Dimova and C. Marques, CRC Press, Taylor & Francis, Boca Raton, 2020, pp. 73–168.
132 K. Berndl, J. Käs, R. Lipowsky, E. Sackmann and U. Seifert, *Europhys. Lett.*, 1990, **13**, 659–664.
133 J. Käs and E. Sackmann, *Biophys. J.*, 1991, **60**, 825–844.
134 J. Käs, E. Sackmann, R. Podgornik, S. Svetina and B. Žekš, *J. Phys. II*, 1993, **3**, 631–645.
135 H. G. Döbereiner, E. Evans, M. Kraus, U. Seifert and M. Wortis, *Phys. Rev. E*, 1997, **55**, 4458–4474.
136 A. Sakashita, N. Urakami, P. Ziherl and M. Imai, *Soft Matter*, 2012, **8**, 8569–8581.
137 E. Sackmann and A. Ben-Shaul, in *Handbook of Lipid Membranes: Molecular, Functional, and Materials Aspects*, ed. C. R. Safinya and J. O. Rädler, CRC Press, Boca Raton, 2021, pp. 1–31.
138 Y. J. Lu, Y. M. Zhang, K. D. Grimes, J. Qi, R. E. Lee and C. O. Rock, *Mol. Cell*, 2006, **23**, 765–772.
139 D. S. Weiss, *Mol. Microbiol.*, 2004, **54**, 588–597.
140 V. W. Rowlett and W. Margolin, *Front. Microbiol.*, 2015, **6**, 478.
141 M. Leaver, P. Domínguez-Cuevas and J. Errington, *Nature*, 2009, **457**, 849–853.
142 R. Mercier, Y. Kawai and J. Errington, *Cell*, 2013, **152**, 997–1007.
143 Y. Briers, P. Walde, M. Schuppler and M. J. Loessner, *BioEssays*, 2012, **34**, 1078–1084.
144 W. Helfrich, in *Giant Vesicles*, ed. P. L. Luisi and P. Walde, John Wiley & Sons, Chichester, 2000, pp. 50–70.
145 M. P. Do Carmo, *Differential geometry of curves and surfaces: revised and updated second edition*, Dover, New York, 2016.
146 D. Marsh, *Biophys. J.*, 2007, **93**, 3884–3899.
147 R. E. Waugh, J. Song, S. Svetina and B. Žekš, *Biophys. J.*, 1992, **61**, 974–982.
148 L. Miao, U. Seifert, M. Wortis and H. G. Döbereiner, *Phys. Rev. E*, 1994, **49**, 5389–5407.
149 D. Deamer, *Nature*, 1985, **317**, 792–794.
150 K. Morigaki and P. Walde, *Curr. Opin. Colloid Interface Sci.*, 2007, **12**, 75–80.
151 N. Urakami, Y. Sakuma, T. Chiba and M. Imai, *Soft Matter*, 2021, **17**, 8434–8445.
152 I. A. Chen and J. W. Szostak, *Proc. Natl. Acad. Sci. U. S. A.*, 2004, **101**, 7965–7970.
153 R. J. Bruckner, S. S. Mansy, A. Ricardo, L. Mahadevan and J. W. Szostak, *Biophys. J.*, 2009, **97**, 3113–3122.
154 J. A. Hamilton, *Curr. Opin. Lipidol.*, 2003, **14**, 263–271.
155 M. Nakano, M. Fukuda, T. Kudo, H. Endo and T. Handa, *Phys. Rev. Lett.*, 2007, **98**, 238101.
156 M. M. Sperotto and A. Ferrarini, in *The Biophysics of Cell Membranes, Springer Series in Biophysics 19*, ed. R. M. Epand and J.-M. Ruysschaert, Springer, Singapore, 2017, pp. 29–60.
157 R. M. Raphael and R. E. Waugh, *Biophys. J.*, 1996, **71**, 1374–1388.
158 B. Fourcade, L. Miao, M. Rao, M. Wortis and R. K. P. Zia, *Phys. Rev. E*, 1994, **49**, 5276.
159 J. Steinkühler, R. L. Knorr, Z. Zhao, T. Bhatia, S. M. Bartelt, S. Wegner, R. Dimova and R. Lipowsky, *Nat. Commun.*, 2020, **11**, 905.
160 R. Lipowsky, *Adv. Biology*, 2021, 2101020.
161 L. D. Landau, E. M. Lifshitz, A. M. Kosevich and L. P. Pitaevski, *Theory of Elasticity*, Elsevier, New York, 3rd edn, 1986.
162 W. Helfrich and W. Harbich, *Physics of Amphiphilic Layers*, Springer, Berlin, 1987.
163 D. P. Siegel and M. M. Kozlov, *Biophys. J.*, 2004, **87**, 366–374.

164 K. M. Nakagawa and H. Noguchi, *Phys. Rev. E*, 2016, **94**, 053304.
165 N. de Lange, J. M. Kleijn and F. Leermakers, *Phys. Chem. Chem. Phys.*, 2021, **23**, 5152–5175.
166 H. G. Döbereiner, J. Käs, D. Noppl, I. Sprenger and E. Sackmann, *Biophys. J.*, 1993, **65**, 1396–1403.
167 M. M. Hanczyc and J. W. Szostak, *Curr. Opin. Chem. Biol.*, 2004, **8**, 660–664.
168 J. Dervaux, V. Noireaux and A. J. Libchaber, *Eur. Phys. J. Plus*, 2017, **132**, 284.
169 K. Morigaki, P. Walde, M. Misran and B. H. Robinson, *Colloids Surf., A*, 2003, **213**, 37–44.
170 R. Smith and C. Tanford, *Proc. Natl. Acad. Sci. U. S. A.*, 1973, **70**, 289–293.
171 T. H. Haines, *Proc. Natl. Acad. Sci. U. S. A.*, 1983, **80**, 160–164.
172 I. A. Chen and J. W. Szostak, *Biophys. J.*, 2004, **87**, 988–998.
173 T. F. Zhu and J. W. Szostak, *J. Am. Chem. Soc.*, 2009, **131**, 5705–5713.
174 I. Buding, A. Debnath and J. W. Szostak, *J. Am. Chem. Soc.*, 2012, **134**, 20812–20819.
175 M. M. Hanczyc, S. M. Fujikawa and J. W. Szostak, *Science*, 2003, **302**, 618–622.
176 M. Kurisu, H. Aoki, T. Jimbo, Y. Sakuma, M. Imai, S. Serrano-Luginbühl and P. Walde, *Commun. Chem.*, 2019, **2**, 117.
177 P. Walde, R. Wick, M. Fresta, A. Mangone and P. L. Luisi, *J. Am. Chem. Soc.*, 1994, **116**, 11649–11654.
178 R. Wick, P. Walde and P. L. Luisi, *J. Am. Chem. Soc.*, 1995, **117**, 1435–1436.
179 F. M. Menger and K. Gabrielson, *J. Am. Chem. Soc.*, 1994, **116**, 1567–1568.
180 K. Takakura, T. Toyota and T. Sugawara, *J. Am. Chem. Soc.*, 2003, **125**, 8134–8140.
181 K. Takakura and T. Sugawara, *Langmuir*, 2004, **20**, 3832–3834.
182 T. Toyota, K. Takakura, Y. Kageyama, K. Kurihara, N. Maru, K. Ohnuma, K. Kaneko and T. Sugawara, *Langmuir*, 2008, **24**, 3037–3044.
183 M. Matsuo, S. Ohyama, K. Sakurai, T. Toyota, K. Suzuki and T. Sugawara, *Chem. Phys. Lipids*, 2019, **222**, 1–7.
184 J. A. Vance and N. K. Devaraj, *J. Am. Chem. Soc.*, 2021, **143**, 8223–8231.
185 M. D. Hardy, J. Yang, J. Selimkhanov, C. M. Cole, L. S. Tsimring and N. K. Devaraj, *Proc. Natl. Acad. Sci. U. S. A.*, 2015, **112**, 8187–8192.
186 R. J. Brea, C. M. Cole and N. K. Devaraj, *Angew. Chem., Int. Ed.*, 2014, **53**, 14102–14105.
187 R. J. Brea, A. Bhattacharya and N. K. Devaraj, *Synlett*, 2017, **28**, 108–112.
188 L. Liu, Y. Zou, A. Bhattacharya, D. Zhang, S. Q. Lang, K. N. Houk and N. K. Devaraj, *Nat. Chem.*, 2020, **12**, 1029–1034.
189 A. Bhattacharya, R. J. Brea, H. Niederholtmeyer and N. K. Devaraj, *Nat. Commun.*, 2019, **10**, 300.
190 A. Bhattacharya, C. J. Cho, R. J. Brea and N. K. Devaraj, *J. Am. Chem. Soc.*, 2021, **143**, 11235–11242.
191 J. M. Castro, H. Sugiyama and T. Toyota, *Sci. Rep.*, 2019, **9**, 165.
192 I. Ivanov, R. B. Lira, T. Y. D. Tang, T. Franzmann, A. Klosin, L. C. da Silva, A. Hyman, K. Landfester, R. Lipowsky, K. Sundmacher and R. Dimova, *Adv. Biosyst.*, 2019, **3**, 1800314.
193 R. Jahn and H. Grubmüller, *Curr. Opin. Cell Biol.*, 2002, **14**, 488–495.
194 L. K. Tamm, J. Crane and V. Kiessling, *Curr. Opin. Struct. Biol.*, 2003, **13**, 453–466.
195 J. C. Shillcock and R. Lipowsky, *Nat. Mater.*, 2005, **4**, 225–228.
196 A. Grafmüller, J. Shillcock and R. Lipowsky, *Biophys. J.*, 2009, **96**, 2658–2675.
197 P. Kuzmin, J. Zimmerberg, Y. A. Chizmadzhev and F. S. Cohen, *Proc. Natl. Acad. Sci. U. S. A.*, 2001, **98**, 7235–7240.
198 S. A. Tatulian, *Biochim. Biophys. Acta, Biomembr.*, 1983, **736**, 189–195.
199 M. A. Morini, M. B. Sierra, V. I. Pedroni, L. M. Alarcon, G. A. Appignanesi and E. A. Disalvo, *Colloids Surf., B*, 2015, **131**, 54–58.
200 E. Chibowski and A. Szcześ, *Adsorption*, 2016, **22**, 755–765.
201 F. Caschera, P. Stano and P. L. Luisi, *J. Colloid Interface Sci.*, 2010, **345**, 561–565.
202 T. Sunami, F. Caschera, Y. Morita, T. Toyota, K. Nishimura, T. Matsuura, H. Suzuki, M. M. Hanczyc and T. Yomo, *Langmuir*, 2010, **26**, 15098–15103.
203 K. Suzuki, R. Aboshi, K. Kurihara and T. Sugawara, *Chem. Lett.*, 2012, **41**, 789–791.
204 R. B. Lira, T. Robinson, R. Dimova and K. A. Riske, *Biophys. J.*, 2019, **116**, 79–91.
205 J. Heuvingh, F. Pincet and S. Cribier, *Eur. Phys. J. E*, 2004, **14**, 269–276.
206 Y. Dreher, K. Jahnke, E. Bobkova, J. P. Spatz and K. Göpfrich, *Angew. Chem., Int. Ed.*, 2021, **133**, 10756–10764.
207 C. K. Haluska, K. A. Riske, V. Marchi-Artzner, J. M. Lehn, R. Lipowsky and R. Dimova, *Proc. Natl. Acad. Sci. U. S. A.*, 2006, **103**, 15841–15846.
208 A. Grafmüller, J. Shillcock and R. Lipowsky, *Phys. Rev. Lett.*, 2007, **98**, 218101.
209 K. Ikari, Y. Sakuma, T. Jimbo, A. Kodama, M. Imai, P. A. Monnard and S. Rasmussen, *Soft Matter*, 2015, **11**, 6327–6334.
210 A. Cordomí, O. Edholm and J. J. Perez, *J. Phys. Chem. B*, 2008, **112**, 1397–1408.
211 A. Kodama, M. Morandi, R. Ebihara, T. Jimbo, M. Toyoda, Y. Sakuma, M. Imai, N. Puff and M. I. Angelova, *Langmuir*, 2018, **34**, 11484–11494.
212 T. Tanaka and M. Yamazaki, *Langmuir*, 2004, **20**, 5160–5164.
213 S. Deshpande, S. Wunnava, D. Hueting and C. Dekker, *Small*, 2019, **15**, e1902898.
214 Y. Sakuma and M. Imai, *Life*, 2015, **5**, 651–675.
215 J. Zimmerberg and M. M. Kozlov, *Nat. Rev. Mol. Cell Biol.*, 2006, **7**, 9–19.
216 J. N. Israelachvili, *Intermolecular and surface forces*, Academic Press, 2015.
217 Y. Sakuma, N. Urakami, T. Taniguchi and M. Imai, *J. Phys.: Condens. Matter*, 2011, **23**, 284104.

218 L. V. Chernomordik, M. M. Kozlov, G. B. Melikyan, I. G. Abidor, V. S. Markin and Y. A. Chizmadzhev, *Biochim. Biophys. Acta, Biomembr.*, 1985, **812**, 643–655.
219 S. Mayor, J. F. Presley and F. R. Maxfield, *J. Cell Biol.*, 1993, **121**, 1257–1269.
220 Y. Sakuma, M. Imai, M. Yanagisawa and S. Komura, *Eur. Phys. J. E: Soft Matter Biol. Phys.*, 2008, **25**, 403–413.
221 Y. Sakuma, T. Taniguchi and M. Imai, *Biophys. J.*, 2010, **99**, 472–479.
222 Y. Sakuma and M. Imai, *Phys. Rev. Lett.*, 2011, **107**, 198101.
223 T. Jimbo, Y. Sakuma, N. Urakami, P. Ziherl and M. Imai, *Biophys. J.*, 2016, **110**, 1551–1562.
224 M. M. Kamal, D. Mills, M. Grzybek and J. Howard, *Proc. Natl. Acad. Sci. U. S. A.*, 2009, **106**, 22245–22250.
225 A. H. Poghosyan and Y. Sh Mamasakhlisov, *Colloids Surf., A*, 2022, **642**, 128681.
226 J. Derganc, *Phys. Biol.*, 2007, **4**, 317–324.
227 A. Tian and T. Baumgart, *Biophys. J.*, 2009, **96**, 2676–2688.
228 Y. Natsume, O. Pravaz, H. Yoshida and M. Imai, *Soft Matter*, 2010, **6**, 5359–5366.
229 H. Terasawa, K. Nishimura, H. Suzuki, T. Matsuura and T. Yomo, *Proc. Natl. Acad. Sci. U. S. A.*, 2012, **109**, 5942–5947.
230 R. Lipowsky and H.-G. Döbereiner, *Europhys. Lett.*, 1998, **43**, 219–225.
231 B. Różycki and R. Lipowsky, *J. Chem. Phys.*, 2016, **145**, 074117.
232 S. Asakura and F. Oosawa, *J. Chem. Phys.*, 1954, **22**, 1255–1256.
233 A. Vrij, *Colloid and Surface Science*, Pergamon, 1977.
234 S. M. Ilett, S. Orrock, W. C. Poon and P. N. Pusey, *Phys. Rev. E*, 1995, **51**, 1344.
235 Y. Caspi and C. Dekker, *Syst. Synth. Biol.*, 2014, **8**, 249–269.
236 A. Roux, G. Koster, M. Lenz, B. Sorre, J. B. Manneville, P. Nassoy and P. Bassereau, *Proc. Natl. Acad. Sci. U. S. A.*, 2010, **107**, 4141–4146.
237 G. Lan, C. W. Wolgemuth and S. X. Sun, *Proc. Natl. Acad. Sci. U. S. A.*, 2007, **104**, 16110–16115.
238 J. Xiao and E. D. Goley, *Curr. Opin. Microbiol.*, 2016, **34**, 90–96.
239 E. Boucrot, A. Pick, G. Camdere, N. Liska, E. Evergren, H. T. McMahon and M. M. Kozlov, *Cell*, 2012, **149**, 124–136.
240 W. T. Snead, C. C. Hayden, A. K. Gadok, C. Zhao, E. M. Lafer, P. Rangamani and J. C. Stachowiak, *Proc. Natl. Acad. Sci. U. S. A.*, 2017, **114**, E3258–E3267.
241 C. M. Chen, P. G. Higgs and F. C. MacKintosh, *Phys. Rev. Lett.*, 1997, **79**, 1579.
242 N. Urakami, T. Jimbo, Y. Sakuma and M. Imai, *Soft Matter*, 2018, **14**, 3018–3027.
243 T. Tanaka, R. Sano, Y. Yamashita and M. Yamazaki, *Langmuir*, 2004, **20**, 9526–9534.
244 Y. Inaoka and M. Yamazaki, *Langmuir*, 2007, **23**, 720–728.
245 Y. Miele, Z. Medveczky, G. Holló, B. Tegze, I. Derényi, Z. Hórvölgyi, E. Altamura, I. Lagzi and F. Rossi, *Chem. Sci.*, 2020, **11**, 3228–3235.
246 Ö. D. Toparlak, A. Wang and S. Mansy, *J. Am. Chem. Soc. Au*, 2021, **1**, 560–568.
247 S. L. Veatch and S. L. Keller, *Biochim. Biophys. Acta, Mol. Cell Res.*, 2005, **1746**, 172–185.
248 R. Lipowsky, *J. Phys. II*, 1992, **2**, 1825–1840.
249 T. Baumgart, S. T. Hess and W. W. Webb, *Nature*, 2003, **425**, 821–824.
250 C. Leirer, B. Wunderlich, V. M. Myles and M. F. Schneider, *Biophys. Chem.*, 2009, **143**, 106–109.
251 M. Andes-Koback and C. D. Keating, *J. Am. Chem. Soc.*, 2011, **133**, 9545–9555.
252 I. Budin and J. W. Szostak, *Proc. Natl. Acad. Sci. U. S. A.*, 2011, **108**, 5249–5254.
253 S. Deshpande, W. K. Spoelstra, M. van Doorn, J. Kerssemakers and C. Dekker, *ACS Nano*, 2018, **12**, 2560–2568.
254 E. R. Rojas and K. C. Huang, *Curr. Opin. Microbiol.*, 2018, **42**, 62–70.
255 E. Boroske, M. Elwenspoek and W. Helfrich, *Biophys. J.*, 1981, **34**, 95–109.
256 P. Peterlin, G. Jaklič and T. Pisanski, *Meas. Sci. Technol.*, 2009, **20**, 055801.
257 M. Mally, P. Peterlin and S. Svetina, *J. Phys. Chem. B*, 2013, **117**, 12086–12094.
258 N. Rodriguez, S. Cribier and F. Pincet, *Phys. Rev. E*, 2006, **74**, 061902.
259 M. Ohno, T. Hamada, K. Takiguchi and M. Homma, *Langmuir*, 2009, **25**, 11680–11685.
260 B. Božič and S. Svetina, *Eur. Biophys. J.*, 2004, **33**, 565–571.
261 B. Božič and S. Svetina, *Eur. Phys. J. E: Soft Matter Biol. Phys.*, 2007, **24**, 79–90.
262 S. Svetina, *Orig. Life Evol. Biosph.*, 2012, **42**, 483–486.
263 O. Y. Zhong-Can and W. Helfrich, *Phys. Rev. A*, 1989, **39**, 5280–5288.
264 J. Von Neumann, in *The Hixon Symposium*, ed. L. A. Jeffress, Wiley, New York, 1951.
265 P. K. Schmidli, P. Schurtenberger and P. L. Luisi, *J. Am. Chem. Soc.*, 1991, **113**, 8127–8130.
266 Y. Shimizu, A. Inoue, Y. Tomari, T. Suzuki, T. Yokogawa, K. Nishikawa and T. Ueda, *Nat. Biotechnol.*, 2001, **19**, 751–755.
267 Y. Kuruma, P. Stano, T. Ueda and P. L. Luisi, *Biochim. Biophys. Acta, Biomembr.*, 2009, **1788**, 567–574.
268 X. Yu, T. Liu, F. Zhu and C. Khosla, *Proc. Natl. Acad. Sci. U. S. A.*, 2011, **108**, 18643–18648.
269 Z. Liu, Y. Zhang, X. Jia, M. Hu, Z. Deng, Y. Xu and T. Liu, *ACS Synth. Biol.*, 2017, **6**, 701–709.
270 A. Scott, M. J. Noga, P. de Graaf, I. Westerlaken, E. Yildirim and C. Danelon, *PLoS One*, 2016, **11**, e0163058.
271 M. Exterkate, A. Caforio, M. C. Stuart and A. J. Driessen, *ACS Synth. Biol.*, 2018, **7**, 153–165.
272 D. Blanken, D. Foschepoth, A. C. Serrão and C. Danelon, *Nat. Commun.*, 2020, **11**, 4317.
273 K. Kurihara, M. Tamura, K. I. Shohda, T. Toyota, K. Suzuki and T. Sugawara, *Nat. Chem.*, 2011, **3**, 775–781.
274 M. Matsuo, Y. Kan, K. Kurihara, T. Jimbo, M. Imai, T. Toyota, Y. Hirata, K. Suzuki and T. Sugawara, *Sci. Rep.*, 2019, **9**, 6916.
275 K. Kurihara, Y. Okura, M. Matsuo, T. Toyota, K. Suzuki and T. Sugawara, *Nat. Commun.*, 2015, **6**, 8352.

276 K. Junker, G. Zandomeneghi, Z. Guo, P. Kissner, T. Ishikawa, J. Kohlbrecher and P. Walde, *RSC Adv.*, 2012, **2**, 6478–6495.
277 S. Połowiński, *Prog. Polym. Sci.*, 2002, **23**, 533–577.
278 J. P. Foreman and A. P. Monkman, *Synth. Met.*, 2003, **107**, 7604–7610.
279 S. Luginbühl, M. Milojević-Rakić, K. Junker, D. Bajuk-Bogdanović, I. Pašti, R. Kissner, G. Ciric-Marjanovic and P. Walde, *Synth. Met.*, 2017, **226**, 89–103.
280 G. Tsuji, S. Fujii, T. Sunami and T. Yomo, *Proc. Natl. Acad. Sci. U. S. A.*, 2016, **113**, 590–595.